

Review

# Advances in P(VDF-TrFE) Composites: A Methodical Review on Enhanced Properties and Emerging Electronics Applications

Lekshmi Priya P S <sup>1</sup>, Biswaranjan Swain <sup>2</sup>, Shailendra Rajput <sup>3</sup> , Saubhagyalaxmi Behera <sup>1,\*</sup> and Sabyasachi Parida <sup>2,\*</sup> 

<sup>1</sup> Department of Physics, Centurion University of Technology and Management, Bhubaneswar 752050, Odisha, India; sanamnair1@yahoo.co.in

<sup>2</sup> Department of Physics, C.V. Raman Global University, Bhubaneswar 752054, Odisha, India; swainbiswaranjan03@gmail.com

<sup>3</sup> College of Engineering, Xi'an International University, Xi'an 710077, China; shailendra@xaiu.edu.cn

\* Correspondence: saubhagyalaxmi.behera@cutm.ac.in (S.B.); sabyasachiparida023@gmail.com (S.P.)

**Abstract:** Piezoelectric polymers are a class of material that belong to carbon–hydrogen-based organic materials with a long polymer chain. They fill the void where single crystals and ceramics fail to perform. This characteristic of piezoelectric polymers made them unique. Their piezoelectric stress constant is higher than ceramics and the piezoelectric strain is lower compared to ceramics. This study's goal is to present the most recent information on poly(vinylidene fluoride) with trifluoroethylene P(VDF-TrFE), a major copolymer of poly(vinylidene fluoride) PVDF with piezoelectric, pyroelectric, and ferroelectric characteristics. The fabrication of P(VDF-TrFE) composites and their usage in a variety of applications, including in actuators, transducers, generators, and energy harvesting, are the primary topics of this work. The report provides an analysis of how the addition of fillers improves some of the features of P(VDF-TrFE). Commonly utilized polymer composite preparation techniques, including spinning, Langmuir–Blodgett (LB), solution casting, melt extrusion, and electrospinning are described, along with their effects on the pertinent characteristics of the polymer composite. A brief discussion on the literature related to different applications (such as bio-electronic devices, sensors and high energy-density piezoelectric generators, low mechanical damping, and easy voltage rectifiers of the polymer composite is also presented.

**Keywords:** polymer; ceramic; composite; PVDF; P(VDF-TrFE)



**Citation:** P S, L.P.; Swain, B.; Rajput, S.; Behera, S.; Parida, S. Advances in P(VDF-TrFE) Composites: A Methodical Review on Enhanced Properties and Emerging Electronics Applications. *Condens. Matter* **2023**, *8*, 105. <https://doi.org/10.3390/condmat8040105>

Academic Editor: Milorad Milosevic

Received: 26 October 2023

Revised: 27 November 2023

Accepted: 28 November 2023

Published: 1 December 2023



**Copyright:** © 2023 by the authors. Licensee MDPI, Basel, Switzerland. This article is an open access article distributed under the terms and conditions of the Creative Commons Attribution (CC BY) license (<https://creativecommons.org/licenses/by/4.0/>).

## 1. Introduction

Piezoelectric materials are widely exploited in electronics and biotechnology for their unique features. Piezoelectric ceramics are widely accepted among the piezoelectric materials because of their strong piezoelectric properties. However, piezoelectric polymer served as a better alternative for piezoelectric ceramic to overcome some of the disadvantage like brittleness, high density, rigidity, stiffness, and high leakage current. Piezoelectric polymers have high dielectric breakdown strength, flexibility, and cost-effective fabrication routes. Even though they have comparatively low piezoelectric coefficient than ceramics, their high mechanical flexibility and biocompatibility help them to find a place in various technical application [1–6].

Numerous studies on piezoelectric polymer composite provide desirable results as they combine the merits of fillers and polymers. They are used to store energy from ambient vibrations as well as for energy harvesting [7]. In addition, these compounds are widely used in different electronic device like sensors, actuators, transducers, and generators. Biological technology gained benefits by fabricating various biological devices which proved to be a boon to the living form.

This review mainly focuses on a particular copolymer, (PVDF-TrFE) and its composite. It mainly emphasis on the most followed technique for the fabrication of polymer composite

film along with their applications. The effect of fillers in the polymer matrix for the improvement of physical and chemical properties are also discussed.

1.1. Piezoelectric Effect

Jacques Curie along with Pierre Curie, in 1880 discovered piezoelectricity, charge generation which is formed due to the deformation of solid material and vice versa. Piezoelectricity is used to describe the coupling amongst electrical and mechanical performance of materials. The word piezo derived from a Greek word meaning to press [8–14]. Gabriel Lippmann (1881) derived the converse piezoelectric effect mathematically from the thermodynamic principle. The same was confirmed by Curie’s very immediately [12]. The piezoelectric effect expresses the linear relationship amongst the mechanical and electrical field that is detected in certain classes of materials. The linear relationship between the output electrical signal and the mechanical stress is given by:  $x = dE$ , where  $d$  is the reverse piezoelectric strain constant,  $E$  is the electric and  $x$  is the strain. Piezoelectricity exists in noncentrosymmetric dielectric materials. When mechanical force is applied, shifting of ions takes place and dipoles are formed. Charges are formed at the two ends of the material due to accumulation of dipoles in a particular direction. The charges thus formed can be made available externally by connecting electrodes to both end of the material. This effect is known as direct piezoelectric effect. The expansion of material resulted in negative charge whereas the compression of material in positive charge. Direct Piezoelectric Effect leads to a particular crystal arrangement with spontaneous polarization [15]. Diagrammatic representation of direct and converse piezoelectric effect is shown in Figure 1. The piezoelectric effect is often signified by linear constitutive equations as given below:

$$S = S^E T + dE \tag{1}$$

$$D = dT + \epsilon^T E \tag{2}$$

where

$S$ : the strain, relative deformation

$S^E$ : compliance, inverse of elasticity, under constant electric field

$T$ : applied stress

$d$ : piezoelectric charge constant

$E$ : applied electric field

$D$ : dielectric displacement

$\epsilon^T$ : dielectric constant under constant stress

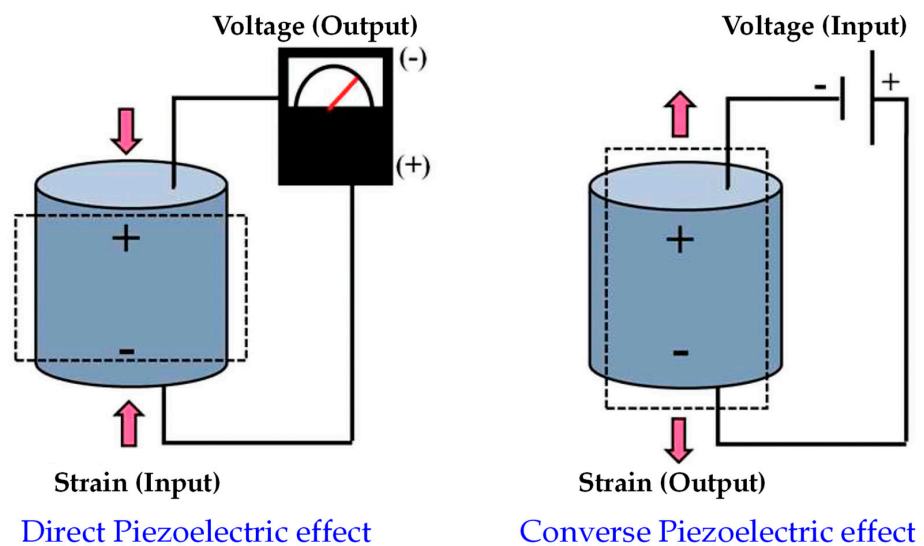


Figure 1. Piezoelectric effect [15].

The piezoelectric materials are classified in different categories depending mainly on the material arrangement and the manufacturing as ceramics, single crystals, and polymers.

### 1.2. Piezoelectric and Ferroelectric Polymer

Piezoelectric polymers are organic compounds with a high molecular weight and long-range order. The materials are more resilient and flexible than those in other classes. They are flexible, tough, lightweight and easily processed. They have high dielectric breakdown and operating field strength with a few limitations, such as low dielectric constant, density, elastic stiffness, and acoustic/mechanical impedance. They are usually semi-crystalline materials with an amorphous matrix. Stretching of these polymers is required to convert nonpolar phase to the polar phase and poling is required for the alignment of the dipoles. Many polymers show polarization hysteresis due to induced polarization. They have a polar unit cell, and an electric field can reverse the direction of its polarization. Polymers like PVDF and copolymers, odd nylons, polyacrylonitrile, polyurea, liquid crystal are some of the more attractive ferroelectric polymers [16–20].

In 1969, Kawai discovered the piezoelectric effect in PVDF film. The ferroelectric property of PVDF was discovered in the late 1970s. Among the polymers, PVDF and its copolymers are widely used for various applications because of their low leakage current, large spontaneous polarization, chemical stability, large dielectric constant, low processing temperature, and flexibility. It is a white crystalline thermoplastic fluoropolymer with a density of 1.78 g/cm<sup>3</sup>. The polymer has a melting point temperature of 171–180 °C. The crystallization temperature lies between 141–151 °C, according to the literature [21]. PVDF exhibits a moderate piezoelectric effect, which can be further enhanced by stretching and polarization. The PVDF polymer is inherently polar and the chemical formula of PVDF is (CH<sub>2</sub>-CF<sub>2</sub>)<sub>n</sub>. In the polymer chain, hydrogen and fluorine atoms are dispositioned symmetrically. This distribution of atoms influences the electromechanical response, solubility, dielectric property, crystal morphology, and dielectric constant. PVDF is chemically inert, tough, and has good stability when exposed to the sun. It has low permittivity and low density. The dielectric constant of PVDF is about 10, which is the highest among the polymers useful for device applications. The glass transition temperature of the amorphous phase is –35 °C, which is below room temperature. PVDF has five crystal phases ( $\alpha$ ,  $\beta$ ,  $\gamma$ ,  $\delta$  and  $\epsilon$ ) [22]. The  $\alpha$ ,  $\beta$ ,  $\delta$  crystal phases are shown in Figure 2. The phases  $\beta$ ,  $\gamma$  and  $\delta$  have a polar nature. The phase, ' $\alpha$ ' can be obtained by casting PVDF from the melt, whereas by stretching the non-polar  $\alpha$  phase at an elevated temperature, it can be changed into a  $\beta$  phase. The  $\delta$  phase can be obtained by rotating the molecular chain axis in the presence of a high electric field. The  $\beta$  phase has an orthorhombic structure with trans-molecule conformation with large spontaneous polarization, resulting in ferroelectric and piezoelectric properties. The phase has a planar zigzag chain with lattice parameters of  $a = 9.12 \text{ \AA}$ ,  $b = 5.25 \text{ \AA}$  and  $c = 2.55 \text{ \AA}$ . The  $\beta$  phase is the only polar phase having polarization along the C–F dipole moment and is perpendicular to the polymer chain direction. In all trans phases, the hydrogen atoms face one direction and the fluorine atoms face the other direction, thus producing a net dipole moment. Due to the mutual repulsion of fluorine atoms, this all-Trans conformation is not stable, and changes occur above the Curie temperature where the thermal kinetic energy is sufficient to cause segmental rotation. The  $\alpha$  phase is a nonpolar phase with molecules in a distorted trans-gauche-trans-gauche' (TG TG') configuration, a state with the lowest energy. In the  $\beta$  phase, all molecules are in all-Trans (TTT) configurations and the polarization of this phase is given in Figure 3. The  $\gamma$  phase is also a polar phase, where the molecules are oriented in (T3GT3G') a configuration with a small dipole moment. The  $\delta$  phase configuration is similar to that of the  $\alpha$  phase but is oriented in a different way. Different processing conditions are used to achieve different phases of P(VDF-TrFE) [23–41].

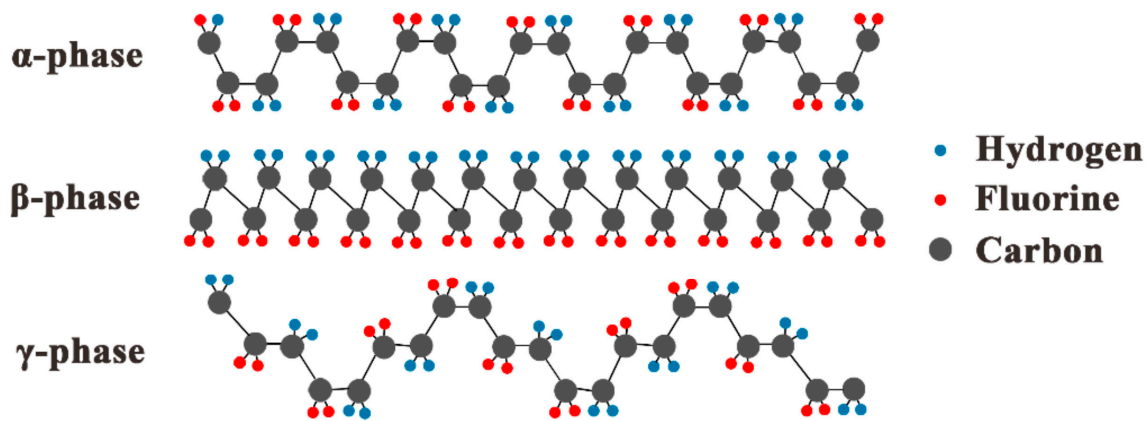


Figure 2. Different crystal phases of PVDF [42].

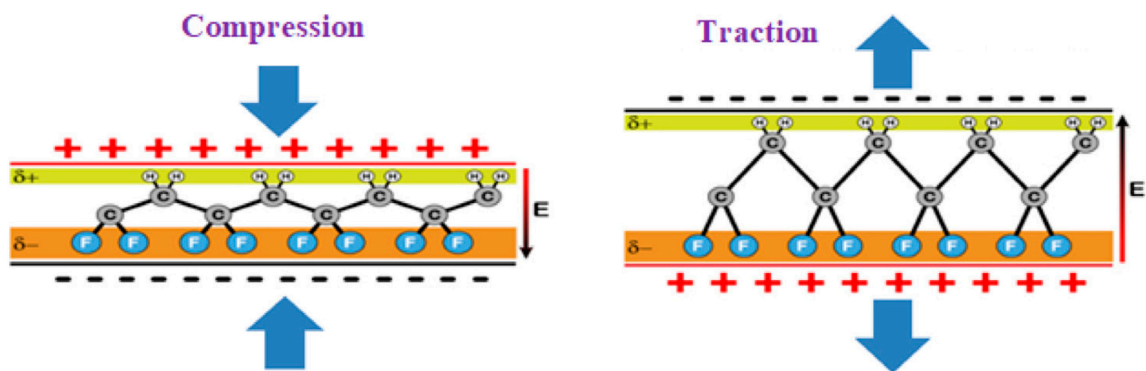


Figure 3. Polarization of  $\beta$  phase on compression and traction [43].

P(VDF-TrFE) is formed by the addition of TrFE ( $-\text{CF}_2-\text{CFH}-$ ) to PVDF, as shown in Figure 4. The interplanar distance and unit cell of the ferroelectric phase is modified by the addition of TrFE. The reduction in the interaction between each cell and dipole results in the lowering of the Curie temperature below melting temperature. The VDF/TrFE ratio is important in determining the phase change and structure of the copolymer. P(VDF-TrFE) crystallizes directly into the  $\beta$  phase. The ferroelectric property of P(VDF-TrFE) originates from the prominent variation in electro-negativity between fluorine, carbon, and hydrogen. The Pauling's value of fluorine is 4, the carbon value is 2.5, and the hydrogen value is 2.1. The fluorine atom attracts all the electrons to its side, thereby creating polarization. The all-trans zig-zag planar configuration contributes to the generation of high polarization along the  $b$  axis. The formation of the phase can be varied through thermal treatments and deposition methods. The concentration of TrFE plays an important role in phase formation. The copolymer has higher remnant polarization and crystallinity than the monomer. The Curie temperature is 116–145 °C, and depends on the composition of VDF/TrFE. The inherent  $\beta$  phase of the copolymer is due to the extra fluorine atom, which in turn improves dielectric property of the copolymer. The interplanar spacing  $b$  is 0.45 nm, and, in the copolymer, ferroelectric to paraelectric change occurs at the Curie temperature. The inherent piezoelectricity of the polymer and copolymer is caused by the highly aligned dipole moments in the crystals. The copolymer has many advantages, such as ferroelectric phase transition, high electromechanical coupling factor, mechanical stability and spontaneous polarization. A comparative study of the dielectric constant and  $d_{33}$  value of different polymers is listed in Table 1 and the P-E loop study of PVDF and the copolymer is shown in Figure 5 [44–60].

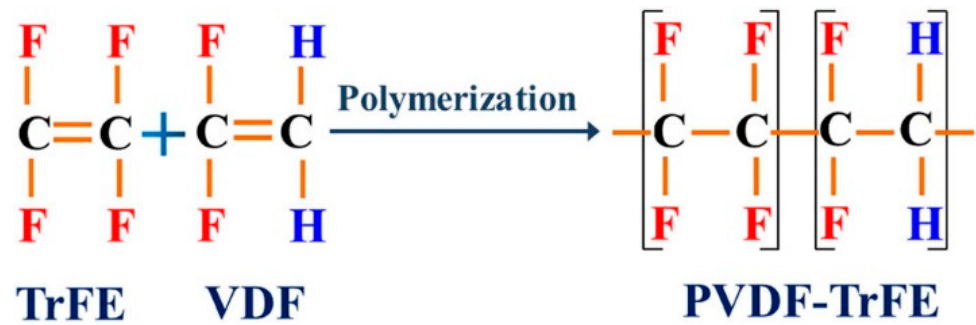


Figure 4. Polymerization of TrFE and VDF [45].

Table 1. Comparative study of  $d_{33}$  and dielectric constant values of different polymers.

Sr No	Polymer	Dielectric Constant	$d_{33}$	References
1	Polyamides	2.78–3.48	2 pC/N	[39,40]
2	Polyurea	5.82	5.51 pm/V	[61–63]
3	Polyvinylidene chloride	5	-	[64]
4	PVDF	10	49.6 pm/V	[65,66]
5	PVDF-CTFE	15(91:9 mol%)	-4 pC/N (18.66 wt% of CTFE)	[65,67]
6	PVDF-HPF(96:4 mol%)	14(96:4 mol%)	17.7 pm/V	[68,69]

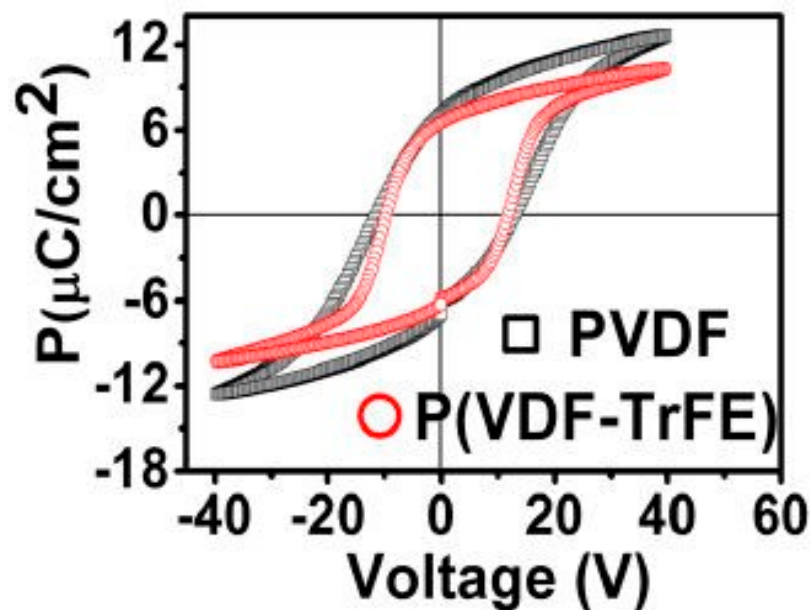
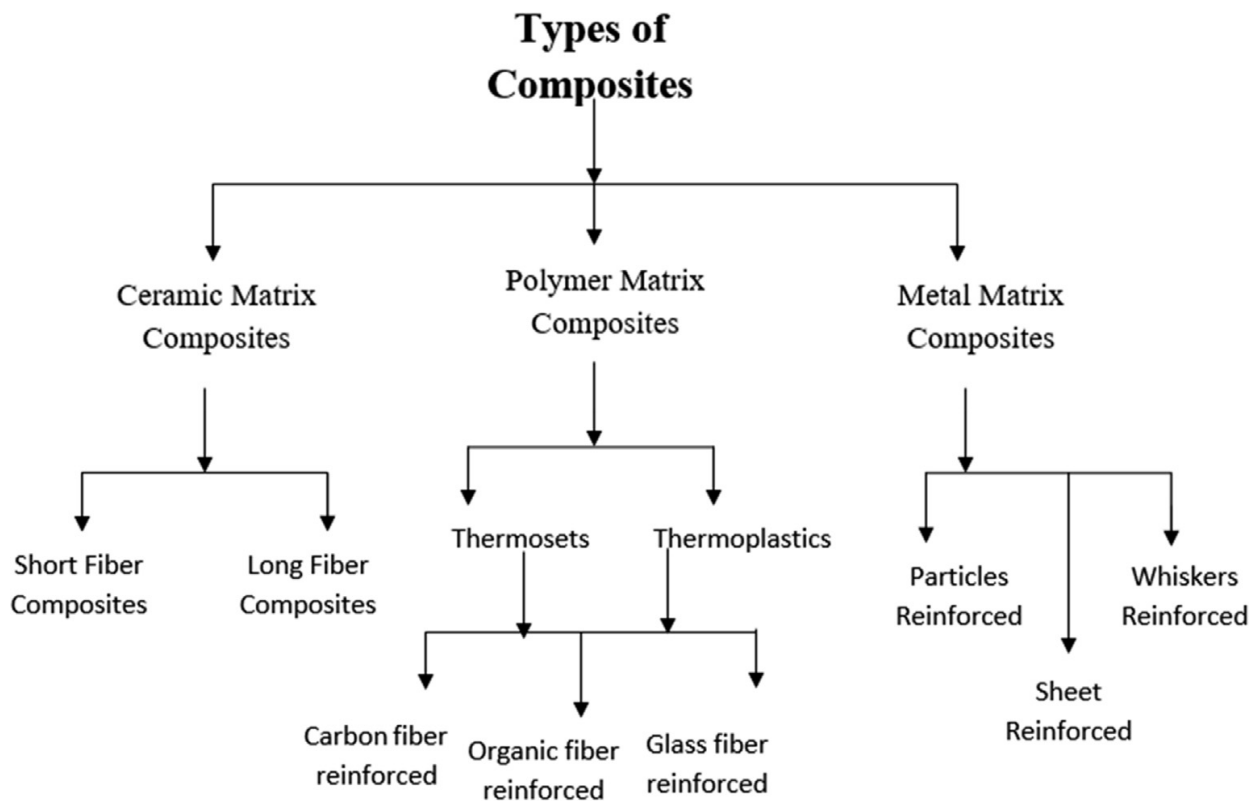


Figure 5. P-E loops of PVDF and P(VDF-TrFE) from LB films [46].

### 1.3. General Mechanism to Enhance the Properties of Polymer

The last two decades have seen widespread studies conducted to improve the properties of polymers. Polymer composite fabrication is studied by various researchers to improve chemical as well as physical properties. Composites are categorized depending upon the types of matrix materials. Glass-fiber-reinforced polymer composites are useful for the manufacturing of plastic and industrial items like pipe, floorings, containers etc. Carbon-fiber-reinforced polymer composites are mainly used whenever there is a need for a high strength-to-weight ratio and stiffness, such as in the aerospace, automotive, and superstructure industries. Carbon fiber reinforcements have very high elasticity and can withstand high temperatures [70]. The different types of composites are illustrated in Figure 6.



**Figure 6.** Types of composites [70].

The addition of functional fillers and reinforcements improves the friction and wear performance of polymer composites. This advantage of polymer composites is used in many industrial applications. Polymer composites can be guided magnetically by controlling the displacement through a magnetic field gradient in a system consisting of magnetic materials associated with a polymeric matrix. It aids, as a multifunctional structure, to bind different species. This approach has proved to be very productive in the biomedical field dealing with cell delivery for diagnostic purposes. Because of their low weight, high strength, toughness, thermomechanical stability, and corrosion resistance behavior, they have found applications in other fields [71]. Newnham et al. presented the concept of connectivity for classifying various ceramic polymer composites. For a two-phase composite, the connectivity can be identified, i.e., if a phase is self-connected in all three directions, then it is called 3 and if it is connected in the Z direction it is called 1. A diphasic composite has 10 types of connectivity (0-0, 1-0, 2-0, 3-0, 1-1, 2-1, 3-1, 2-2, 3-2, 3-3). If the self-connection is only in the Z direction it is called 1 and if the X, Y, and Z directions are self-connected, it is called 3. The 0-0 composite comprises two alternating hatched and unhatched cubes. Phase 1 is connected along the Z direction in a 1-0 composite, whereas fillers are arranged in a three-dimensionally connected polymer matrix. The 3-1 composite is a honeycomb-shaped filler that contains a one-dimensionally connected polymer base. In the 2-2 composite, fillers and polymer sheets are stacked alternatively. Several research studies have demonstrated the enhancement of dielectric behaviors, and the piezoelectric and ferroelectric properties of P(VDF-TrFE) after the addition of fillers into a polymer matrix [72–76]. The addition of a third conductive phase to the polymer is also a method to increase the conductivity of the composite, which in turn increases polarization to the desired extent [77,78]. Two-phase composites with respect to connectivity are presented in Figure 7.

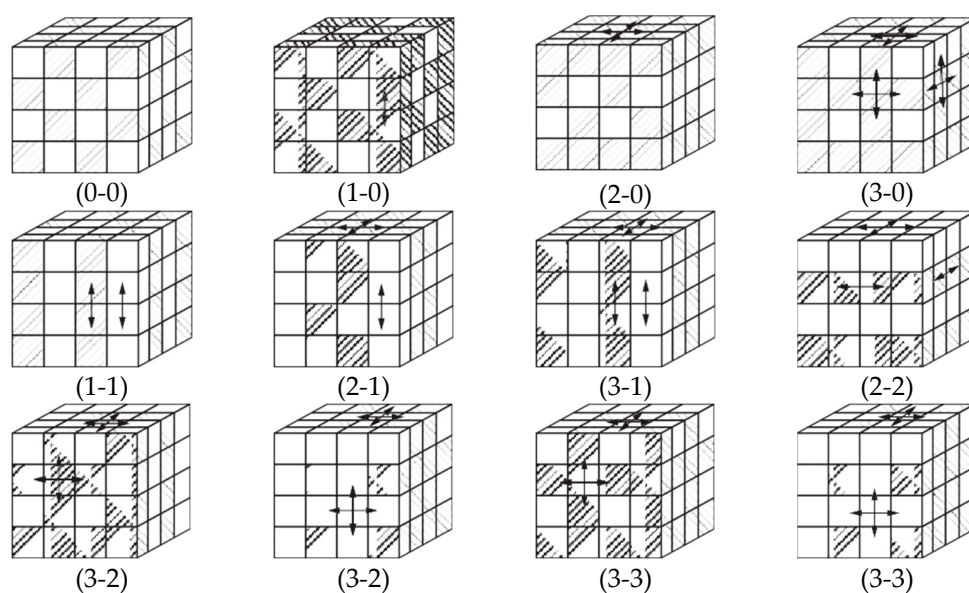


**Figure 7.** Two-phase composites with respect to connectivity [73].

A literature review showed that the piezoelectric and ferroelectric properties can be altered by the inclusion of fillers as well as a third conductive phase. In a 1-3 composite, the polymer composite is randomly arranged as rods in the film, whereas in 0-3, the nanoscale fillers are arranged in a matrix. For 3-3 composites, the particle is well-separated and not in contact. This article presents an overview of current advances in P(VDF-TrFE) composites. The main focus of review is on the most followed synthesis techniques of P(VDF-TrFE) composites and the changes in properties of the composites compared to that of polymer and fillers. The article has highlighted morphological changes, the influence of individual phases, the solvents used, variations in results, and the application of P(VDF-TrFE) composites in different technologies.

## 2. Synthesis Methods of P(VDF-TrFE) Composite and Their Applications

The literature focusing on the preparation of two- and three-phase PVDF-TrFE composites using different processing techniques has highlighted a wide improvement in the physiochemical properties of the composite. Researchers have shown extensive interest in studying the effects of the inclusion of fillers/nanofillers to enhance the  $\beta$  phase of the copolymer P(VDF-TrFE) along with other physiochemical properties. This paper focuses on studies where commonly used synthesis methods of polymer composites, like the spin-coating method, solution casting method, LB method, and melt extrusion were used and the effects of the inclusion of a second phase like zinc oxide(ZnO), magnesium oxide(MgO),  $\text{Bi}_{0.5}\text{Na}_{0.5}\text{TiO}_3$ (BNT),  $\text{BaTiO}_3$ , polydopamine-modified  $\text{BaTiO}_3$ , calcium-modified lead titanate,  $\text{La}_{0.7}\text{Ba}_{0.3}\text{MnO}_3$ ,  $\text{CaCuTi}_4\text{O}_{12}$ , and BCZT on their physical as well as chemical properties. According to the literature, the substrates generally used by researchers for the fabrication of various power devices along with the copolymer include  $\text{SiO}_2$ ,  $\text{Al}_2\text{O}_3$ , pyrolytic graphite, polyamide, and stainless steel. This review mainly focused on the improvement of parameters, such as the dielectric, piezoelectric and ferroelectric properties of the polymer composite and the favorable utilization of these changes in various applications. We also discuss recently reported studies regarding applications of the polymer composite, such as sensor, energy harvesters, nanogenerators, transducers, resonators, and biomedical applications.

### 2.1. Composite Prepared from Spin-Coating Method

The spin-coating method has become one of the main choices in the preparation of films by researchers in various fields owing to its good results, simple procedure, and

comparatively inexpensive instruments. It is the simplest method for the fabrication of uniform thin films in substrates with thicknesses varying from micro- to nanometers. The spin-coated film consists of large crystalline grains and their molecular axes are arranged parallel to the film's surface. A diagrammatic representation of the spin-coating method is shown in Figure 8. P(VDF-TrFE) composites synthesized by the spin-coating method have a wide range of applications in different fields of technology, such as sensing and transducing technologies, because of their uniformity and thickness. Research on P(VDF-TrFE) composites encompassing this method mainly focus on changing various parameters, including the annealing temperature and speed of spin-coating for better results [79–81].

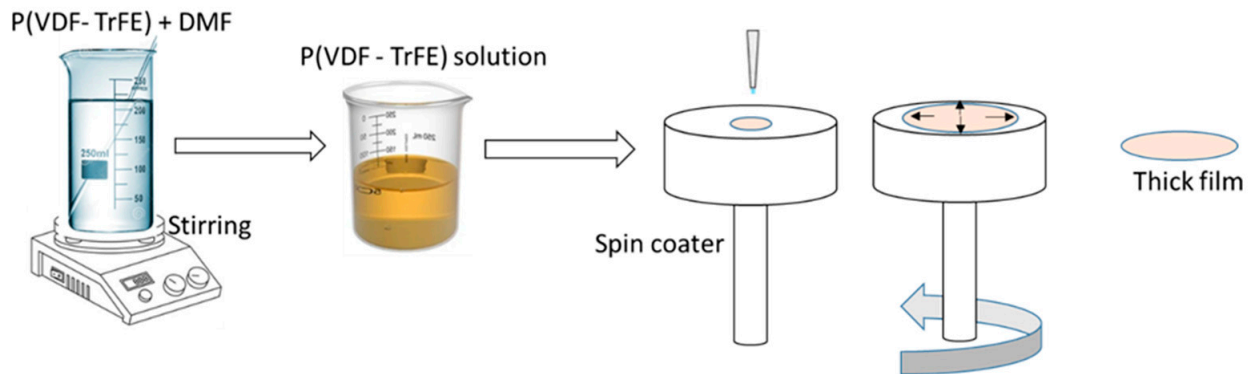


**Figure 8.** Diagrammatic representation of spin-coating method.

Dahan et al. [82] prepared spin-coated single and bilayer 0–3 film of P(VDF-TrFE) dissolved in zinc oxide dispersed methyl ethyl ketone (MEK). The methodology included the dissolution of P(VDF-TrFE) and zinc oxide on MEK individually. Various load percentages of ZnO were dissolved in a P(VDF-TrFE) solution and stirred for 24 h. The single layer and bilayer solutions were spin-coated on an Al substrate at 1500 rpm for 90 s. For the bilayer preparation, the solution was annealed at 80 °C for 10 min before spin-coating. The thickness of the film obtained for 3% of the ZnO loading was 241 nm for a single layer and 316 nm for bilayer. The 3% loading film had a relatively high  $\beta$  phase. The study displayed improved resistivity properties for a minor loading percentage of ZnO fillers. For 3 wt%, the resistivity property was  $3.42 \times 10^5 \Omega \text{ cm}$  for a single layer and two times that of the single layer resistivity for the double layer. The enhancement of resistivity resulted in its utilization in a storage device as a dielectric film. The thermal treatment method for organization of  $\beta$  phase P(VDF-TrFE) was studied by Lau et al. [83]. The P(VDF-TrFE) (70:30 mol%) powder was dissolved in butan-2-one to obtain a solution with a 1 wt.% concentration. The solution was spin-coated onto an Au sputtered glass slide. The film was annealed at 125 °C, 150 °C and 80 °C for 4 h in an oven and then allowed to cool to room temperature. The crystallinity of P(VDF-TrFE) was increased by annealing at a temperature between the Curie temperature and melting point. The increase in annealing temperature changed the grain size from relatively small to coalesce at a grain size of 160 nm at 150 °C. The chain mobility was higher in the paraelectric phase compared to the ferroelectric phase. The morphology of the film annealed below the melting point showed edges on crystalline lamellae grains whereas the grain size enlarged with increases in temperature. The study of the influence of various annealing temperatures on the morphology of P(VDF-TrFE) by Rozana et al. [84] demonstrated needle-like crystallite at the melting point. The film was prepared by dissolving P(VDF-TrFE) of 70:30 mol% in methyl ethyl ketone and stirred for 24 h followed by sonication for 1 h using an ultrasonic bath. The thickness of the film was 150 nm. The film annealed at the Curie temperature had a distinct crystalline structure and a dielectric constant of 7.8 at  $10^4 \text{ Hz}$  was obtained for the film recrystallized at  $T_C$ . Tingting et al. studied the property enhancement of P(VDF-TrFE) films with a formation of two 0-3 composites, BaTiO<sub>3</sub>/P(VDF-TrFE) and polydopamine-modified BaTiO<sub>3</sub>/P(VDF-TrFE) films using spin-coating methods [85]. The dried films

(60 °C for 4 h) were annealed at 140 °C for 24 h. The study showed an improvement in the  $\beta$  phase and crystallinity by adding BaTiO<sub>3</sub>(BT) and polydopamine-modified BT. The size of the nanofillers were 35.9 nm and 39.4 nm for BaTiO<sub>3</sub>/P(VDF-TrFE) and polydopamine-modified BaTiO<sub>3</sub>/P(VDF-TrFE), respectively. The enhancement of the  $\beta$  phase was due to the induced TTTT chain packing of the copolymer because of the presence of polar -OH on the polydopamine. The comparative investigation of the structural and ferroelectric properties of PVDF and P(VDF-TrFE) (72:28) thin film (1.1  $\mu$ m) by the spin-coating method was conducted by Chen et al. [86]. To improve the  $\beta$  phase of PVDF, Mg (NO<sub>3</sub>)<sub>2</sub> 6H<sub>2</sub>O was added to the polymer. The addition of hydrated salt made all-Trans conformation more promising for PVDF, with the hydrogen atom bonding between the water for crystallization. A morphology study showed that the dense surface of the PVDF was due to tiny granular features from the hydrated salt. The P(VDF-TrFE) had crystallized to a rod-like shape consisting of multiple stacks of lamellar crystals with gaps between them. The properties of PVDF and its copolymer P(VDF-TrFE) are listed in Table 2 and show that low-cost PVDF homopolymers can be used as a substitute for P(VDF-TrFE). The study also showed that the  $P_r$  and  $E_C$ , at 150 °C, are 7.5  $\mu$ C/cm<sup>2</sup> and 15 V, respectively.

**Table 2.** Properties of P(VDF-TrFE) [86].

Property	PVDF	P(VDF-TrFE)
Dielectric constant (1 kHz at 25 °C)	12.5	13.2
Dielectric loss	0.031	0.023
d <sub>33</sub> (pC/N)	−15	−17.8
Breakdown Strength (MV/m)	523 ± 25	402 ± 25

Park et al. [87] reported on spin-coated epitaxially grown P(VDF-TrFE) thin films on polytetrafluoroethylene substrates. The morphological study indicated the crystal formation of a substantially ordered structure with its chain-axis parallel to that of PTFE. Hafiz et al. [88] studied a spin-coated 0-3 phase P(VDF-TrFE) film with MgO. An increase in MgO to the matrix produced a drop in crystallinity and a shift in the XRD peak from 19.20 to 17.50 from 5% to 7% at 1200 °C, depicting the  $\alpha$  phase presence in the film. At a 3% loading of MgO, the presence of these fillers acted as a hindrance and obtained fine packing of crystalline in the form of elongated packed crystalline, resulting in low-porosity films. The film exhibited an elevated dielectric constant value (13.7 at 1 kHz) compared to the unfilled copolymer. However, the ferroelectric and dielectric characteristics above the 3% MgO loading of the composite decreased due to agglomeration. The pyroelectric and ferroelectric properties of a P(VDF-TrFE)-Bi<sub>0.5</sub>Na<sub>0.5</sub>TiO<sub>3</sub> nanocomposite spin-coated film, annealed at 100 °C, showed the presence of the  $\beta$  phase, as shown in the study by Mahdi et al. [76]. The P(VDF-TrFE)-Bi<sub>0.5</sub>Na<sub>0.5</sub>TiO<sub>3</sub> nanocomposite reported large rod-like crystal grains and agglomeration when the volume of BNT was increased to 0.30. With the increase in BNT particles, the dielectric value started to increase due to the increment in the dielectric constant of BNT and was approximately 15.5 for a BNT volume fraction of 0.2. The remnant polarization of the copolymer also increased for the volume fraction of 0.2 of BNT. The fast-switching speed of the capacitor from downward polarization to upward polarization supported the conclusion that graphene electrodes provide fast polarization switching when used in an ferroelectric capacitor. The dielectric layer's influence on the ferroelectric switching of spin-coated P(VDF-TrFE) film was investigated by Manfang et al. [89]. The dielectric layer of Al<sub>2</sub>O<sub>3</sub> grown thermally above the Al bottom electrodes and the characteristics with different thickness were studied, indicating that, with the increase in thickness of the Al<sub>2</sub>O<sub>3</sub> layer, the hysteresis loop tends, indicating a decrease in the polarization layer with the oxide layer. The negative slope in the hysteresis loop indicates a region where differential capacitance is negative during switching. The ferroelectric can operate in a negative capacitance regime due to the shift in the switching point. The depolarization can cause the shift in the switching point. With the increase in the dielectric layer, the polarization became broader and the switching time also increased.

Yang et al. [90] studied the shear stress induced enhancement of piezoelectric properties of P(VDF-TrFE) films during high spin rate. With the increased spin speed, the grain size progressively grown to a particular direction due to more shear stress and at 6000 rpm where the film revealed the largest grain size with a different orientation. The piezoelectric property which increases with spin rate started to degrade with excessive spin rate owing to dipole alignment degradation and crystallinity. The piezoelectric coefficient amplified about 138% by optimizing the speed of spin coating and the remnant polarization also increased showing highest  $2P_r$ . The influence of cluster size and surface functionalization of ZnO nanoparticle in the thermomechanical and piezoelectric properties of P(VDF-TrFE) 0-3 nanocomposite film prepared by spin-coating method was studied by Nguyen et al. [91]. The young's modulus of the polymer was at  $\sim 1.6$  Gpa at 25 °C and 4.5 Gpa at  $-90$  °C. The enhancement in mechanical properties with increase in volume of nanoparticle may be due to strong interfacial interaction amongst the nanoparticles and P(VDF-TrFE). A decrease of 6% in storage modulus was observed at temperature  $-90$  °C and 25 °C with addition of ZnO (30 wt%) compared to that of 10 wt%. The area of interphase between nanoparticles and the matrix decrease with the increase in cluster size, and hence the reinforcement effect of nano particles was lesser. The  $d_{33}$  value increased with increase in weight percentage of ZnO up to 30 wt% as listed in Table 3.

**Table 3.** Piezoelectric coefficient of 3- $\mu$ m spin-coating films for P(VDF-TrFE) and P(VDF-TrFE)/ZnO [91].

Sample	$d_{33}$ (pC/N)
P(VDF-TrFE)	21
P(VDF-TrFE)/ZnO (1)	21
P(VDF-TrFE)/ZnO (3)	22
P(VDF-TrFE)/ZnO (4)	19

The degradation and nanopatterning of P(VDF-TrFE) thin films fabricated by spin-coating were studied by Zhu et al. [92]. The  $\beta$  phase of P(VDF-TrFE) transformed into a paraelectric intermediate lattice upon irradiation with 100 eV electron radiation and then transformed to an amorphous lattice subsequently. The work reported irreversible degradation of ferroelectricity due to medium-energy electron irradiation ( $<10$  keV). The first-order electromechanical coupling in the P(VDF-TrFE) showed that films became non-ferroelectric after metal deposition in an electron beam evaporator and the degradation process was slowed down by lowering the energy. The polydimethylsiloxane/P(VDF-TrFE) blended film with embedded polystyrene fabricated by Zhang et al. [93] for an electro0wetting device showed an enhancement in dielectric and hydrophobic properties. The roughness of the composite increased with the weight percentage of polydimethylsiloxane to 25 wt%, after which it indicated decrements, showing a supersaturated state and that excess would be precipitated. Polystyrene has a heterogeneous nucleation effect on the copolymers, which increases the nucleation temperature of crystal and hinders crystal growth. The melting temperature shifts to the lower side upon the addition of polydimethylsiloxane, whereas the Curie temperature of the polymer remains unchanged.

Usman et al. studied [94] the effect of surface-treated multi-walled carbon nanotubes (MWCNT) (15 mg, 35 mg, and 55 mg) and BaTiO<sub>3</sub> (5 mL) nanoparticles on the dielectric properties of a P(VDF-TrFE) matrix. Spin-coated three-phase films of different weight percentages (0.01, 0.03, 0.05) of single-walled carbon nanotubes (SMWCNT) with BaTiO<sub>3</sub> in polymer were prepared. The XRD of 0.01 and 0.03 wt% of MWCNT showed no significant changes in the crystal quality of P(VDF-TrFE) after the addition of MWCNT due to the formation of an insulation layer on the surface of MWCNT. The dielectric value of 0.03% showed the highest value of 71 at 1 kHz as the dipoles have enough time to align and hence obtain a high value. The dielectric loss of 0.03 wt% was 0.045 at 1 KHz. A stable and suitable barrier junction was formed on the surface covering of the surface-treated BaTiO<sub>3</sub> and MWCNT and sustained the charges by forming a thick insulation layer. The insulation layer increases the resistance of the thin film by imparting OH groups, which decreases the

dielectric loss and increases the breakdown strength of the material. Marco et al. fabricated a spin-coated P(VDF-TrFE)/CoFe<sub>2</sub>O<sub>4</sub> nanocomposite [95]. Upon subsection of DC magnetic poling at 50 mT the nanocomposite reported  $d_{33}$  of 39 pm/V. The increase in the value can be attributed to the strong interaction between the chain of the nanocomposite and the magnetic field as well as the drag effect produced by the filler used.

Wang et al. studied the trifluoroethylene bond enrichment in P(VDF-TrFE) copolymers by plasma fluorination on bottom electrodes of P(VDF-TrFE)-metal-ferroelectric-metal capacitor [96]. The capacitor shows a charge trapping level of 0.154–0.22 eV emission at 213–273 K for the bottom electrode compared to that of top electrode because of passivation of deep traps by fluorine atoms that diffused from N-type silicon wafers. The  $\beta$  phase of bottom of the polymer film led to the asymmetric remnant polarization and negative internal bias field. The treatment of CF<sub>4</sub> for 1 min gave  $2P_r$  of 6.55  $\mu\text{C}/\text{cm}^2$  and  $E_c$  of 0.47 mV/cm making it suitable for nonvolatile memory applications. Yoonho et al. studied the enhancement of the ferroelectric properties of P(VDF-TrFE) (70/30) films from Nb nanopin electrodes and Nb films [97]. The P(VDF-TrFE) spin-coated film of 200 nm prepared with methyl ethyl ketone as solvent was deposited over the Nb array as well as on Nb thin films. The thin film developed showed the formation of the  $\beta$  phase. The use of an Nb nanopin showed improvement in the ferroelectric property. The formation of nanotemplates of P(VDF-TrFE)/Nb nanopin/SiO/Si substrate and the characterization of the film are shown in Figures 9 and 10.

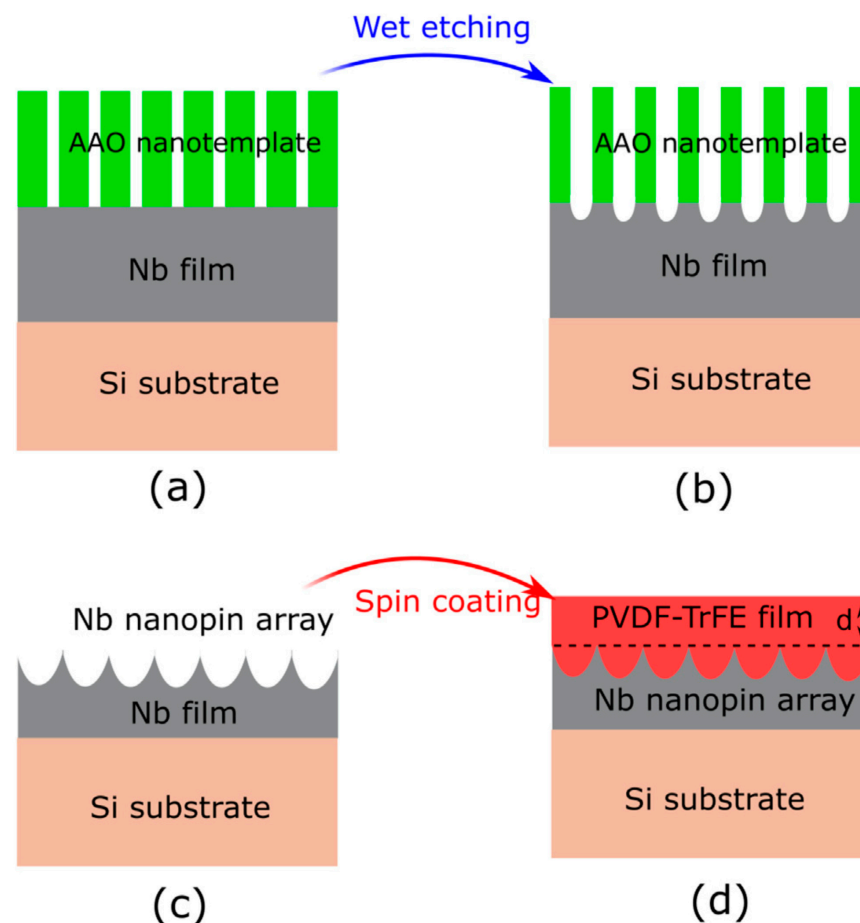


**Figure 9.** (a–c) forming process for Nb nanopin electrodes using an AAO nanotemplate method; and (d) P(VDF-TrFE)/Nb nanopin/SiO/Si substrate-spin-coating technique [97].

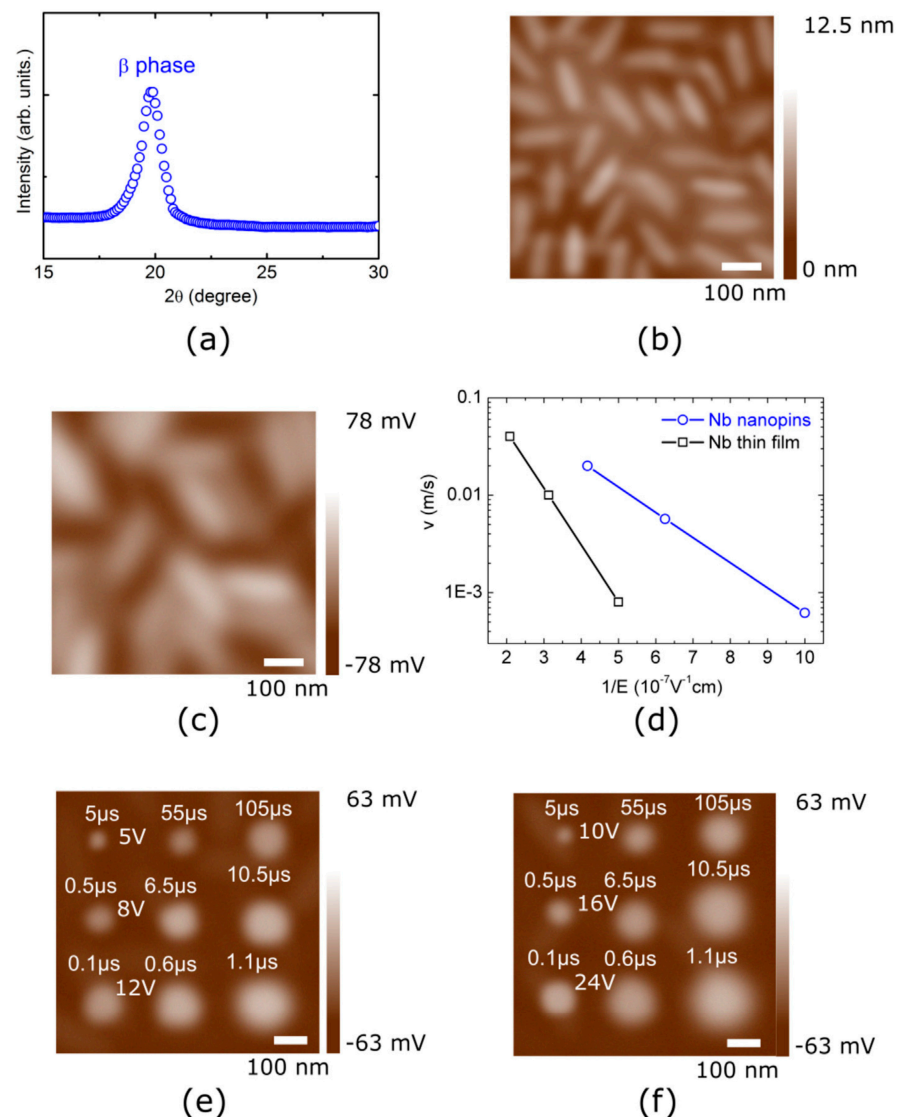


**Figure 10.** (a) XRD of the P(VDF-TrFE) Film; (b) AFM image of the P(VDF-TrFE) film; (c) PFM image of the P(VDF-TrFE) film; (d) domain wall speed vs. inverse applied electric field curves of the P(VDF-TrFE) films; (e) PFM images of ferroelectric polarization bits switched by 5, 8, and 12 V bias with pulse widths for the P(VDF-TrFE) thin film with Nb nanopin electrode; and (f) PFM images of ferroelectric polarization bits switched by different voltage biases with pulse widths for the P(VDF-TrFE) film with Nb thin-film electrode [97].

Spin-coating method is an extensively used method for MEMS fabrication owing to its compatible nature and traditional fabrication method. Research studies showed that the thickness of the film depends on the spin speed and concentration of the solution. The  $\beta$  phase concentration of the film is improved by adjusting various parameters such as the rotational speed, increasing the temperature of substrate, and other post-treatment methods. The selection of solvents with high dipole moments enhances the piezoelectric properties of the prepared film.

### 2.2. Composite Prepared from Solution Casting Method

In the solution casting method, to obtain a viscous solution, the polymer is dissolved in a suitable solvent. This viscous solution is poured onto a flat or non-adhesive surface. The solvent is permitted to evaporate, and the dry film is peeled out from the flat surface. The solvent evaporates at room temperature or above. Small-scale polymers can be prepared by

scattering the polymer solution over a glass surface and being rolled with a glass rod. For large-scale preparations, the solution is fed through a slit die, which is passed in between two oppositely rotating metal drums. The diagrammatic representation of the solution casting method is given in Figure 11.

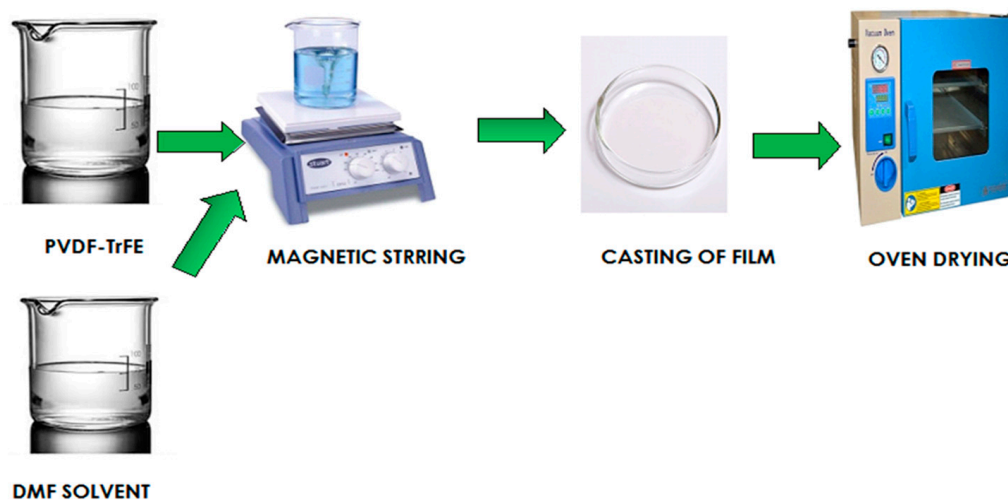


**Figure 11.** Diagrammatic representation of solution casting method.

The solvents are evaporated during rotation and the dry film of the polymer is formed. The solution casting method is based on Stoke's Law. This method is widely used for the preparation of PVDF copolymer-based composite films. Various studies of this method indicate that a temperature above 70 °C is rarely required for the dissolution of the copolymer in the organic solvent. However, in the absence of spontaneous dissolution, ultrasonication and stirring can be applied [98–102]

A nanocomposite film of P(VDF-TrFE) embedded in  $\text{La}_{0.7}\text{Ba}_{0.3}\text{MnO}_3$  (30  $\mu\text{m}$ ) (LBMO) was fabricated by Korner et al. [103]. The nanoparticle was dispersed in the copolymer solution and was cast to a glass plate. The study showed a dielectric constant of approximately 7 for the 0-3 composite with a 15% volume fraction of LBMO at 100 Hz. The  $\text{CaCuTi}_4\text{O}_{12}$ -P(VDF-TrFE) 0-3 nanocomposite [104] exhibited a giant dielectric constant 62 for 50% CCTO and a loss of 0.05 at room temperature at 1 kHz. A composite of novel BCZT,  $\text{Ba}_{0.95}\text{Ca}_{0.05}\text{Ti}_{0.8}\text{Zr}_{0.2}\text{O}_3$ /P(VDF-TrFE) [47] 0-3 composite prepared by the solvent casting method and hot-pressing method showed a high dielectric constant near 90 and a dielectric loss down to 0.024 at 1 kHz for a BCZT volume fraction of 0.4. The study revealed that an increase in filler fraction induces greater space charge, which in turn increases the dielectric constant and loss at a low frequency, whereas at a high frequency both parameters decrease due to the relaxation of the copolymer. A 40  $\mu\text{m}$  film formed by polydopamine-coated barium titanate/P(VDF-TrFE) 0-3 nanocomposite [48] showed an increase in dielectric constant with the addition of  $\text{BaTiO}_3$  and a decrease in the breakdown field. The introduction of polydopamine increased the breakdown strength. A dielectric constant of 46.4 was obtained for 100 Hz with a dielectric loss of 0.07 for 15 wt% of the nanocomposite due to the strong interfacial compatibility raised due to the hydrogen bond between the polydopamine segment and molecular chain. The energy density of 3.3  $\text{J}/\text{cm}^3$  at 225  $\text{MV}/\text{m}$  for 5 wt% of the composite film was attributed to the large content of the electroactive phase and interfacial polarization.

Pereira et al. fabricated P(VDF-TrFE) film using green solvent (1,3 dioxolane(DXL)) by solvent casting method [49]. The comparison study of green film using DMF solvent reported no change in mechanical and thermal properties. The piezoelectric and dielectric responses were not affected by the solvent and evaporation time. The green samples were characterized by dielectric constant of 11 and piezoelectric coefficient  $-21$   $\text{pC}/\text{N}$  which are stable over time and temperature till 100 °C. The interface-dominated time-dependent

behavior of BaTiO<sub>3</sub>/P(VDF-TrFE) composite and its time dependence on 0-3 composite films prepared by solvent casting method consisting of 15 vol.% and 60 vol.% of pristine ceramic particles amino silane and fluoro silane was studied by Dalle et al. [50]. The materials were poled with two different poling procedures. In the first method of poling, the field was applied for 30 min at 110 °C for 1 h, whereas the cooling down was done for approximately 30 °C. In the second method, the electric field was switched off during the 1 h period and cooled for about 30 °C. The time dependence of  $d_{33}$  of P(VDF-TrFE) and composites with 15 vol.% of BaTiO<sub>3</sub>, poled at 100 kV/cm at 110 °C for 30 min and further cooling at room temperature for 60 min was reported to be  $-3$  to  $-2$  pC/N for 100 days. The 15 vol. % of the BaTiO<sub>3</sub> composite film was reported to be a  $d_{33}$  value of 1 to 3 pC/N initially, but changed within the first day to  $-1$  to  $-3$  pC/N. For 60 vol%, the  $d_{33}$ , measured within the first 5 min from the first poling method, was between 25 and 28 pC/N, which decreased and was 10 pC/N for all composites after 100 days at room temperature. The improvement of the ferro- and piezoelectric properties of hydrogenated P(VDF-TrFE) film by annealing at elevated temperature was studied by Wang et al. [51]. Films with a thickness of 10–20  $\mu\text{m}$  were prepared via the casting method and annealed at various temperatures. The absorption intensity showed no visible change by annealing the film at elevated temperatures. With respect to its low cost, facile fabrication conditions, the hydrogenated P(VDF-TrFE) copolymer VDF/TrFE 80/20 (mol%) provided good dielectric and piezoelectric properties. The fabrication of a quasi-two-dimensional neat  $\alpha$  phase P(VDF-TrFE) film in a AlOX/Al-coated SiO<sub>2</sub>/Si substrate was conducted by Qian et al. [52]. A study of the morphology showed that the film exhibited a polycrystalline phase with a grain size of 30 nm and roughness of 0.76 nm. The  $d_{33}$  value was reported to be 46.14 and 41.7 pm/V for  $\alpha$  phase and  $\beta$  phase, respectively, with coercive voltage values of (+3.7,  $-2.3$ ) and (+2,  $-3.6$ ) V.

The solution casting method mainly depends on the temperature of dissolution. Room temperature is not ideal sometimes, and sonication for several hours is required. The increase in the temperature of the evaporation of solvents will increase the crystallinity and  $\beta$  phase. Studies have pointed out that the permittivity of the film increases due to the increase in temperature and the conductivity of the composite film only depends on the amount of filler added.

### 2.3. Composite Prepared from Langmuir–Blodgett Method

The Langmuir–Blodgett method technique is used to prepare ultrathin organic, metal–organic, and polymer layers. The Langmuir films are two- or three-dimensional monomolecular assemblies, amphiphilic molecules at the air–water interface or on the water’s surface. These molecules possess a hydrophobic tail and head and can be arranged at the liquid–gas interface. The water-soluble amphiphilic molecules are spread onto an aqueous phase resulting in partial solubilization of the head group. The process includes the application of pressure using a barrier in a Langmuir trough to achieve a film with the desired combination. The film undergoes a series of phase transitions to finally result in a highly ordered film. The properties of the film largely depend on the substrate used to transfer the Langmuir films. The transfer is conducted by dipping the substrate vertically through the spread monolayer at a constant pressure. The quality of the film largely depends on the parameters, like the PH value of the sub-phase, temperature, speed of dipping, manner of dipping the material, surface pressure of lifting, and speed of compression of the barrier [53,105–107]. A diagrammatic representation of the LB method is shown in Figure 12.

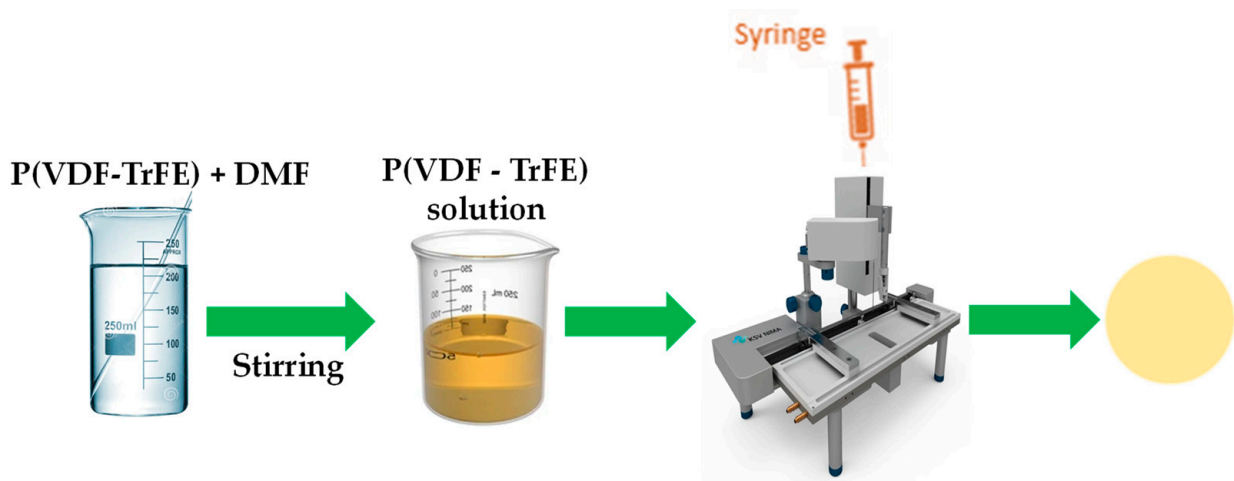


**Figure 12.** Diagrammatic representation of LB method.

The effects of external electric field on the ferroelectric–paraelectric phase transition of P(VDF-TrFE) polymer Langmuir–Blodgett film by Poulsen et al. [53] showed an increase in transition temperature with increases in the applied field. The sample showed a decrease in  $\beta$  phase at a bias of 11.25 V and saturation at 20 V. At 15 V, the paraelectric peak intensity increases with an increase in the ferroelectric peak. The measurement obtained points to the fact that all trans (ferroelectric phases) can be obtained by applying an external field of 265 MV/m. On removal of the electric field, the film returns to a paraelectric state. The zero-field phase transition temperature of the P(VDF-TrFE) was decreased whilst using the LB deposition method. A comparison of the electrocaloric and pyroelectric application of LB-deposited and spin-coated P(VDF-TrFE) was studied by Lindemann et al. [54]. The diffraction pattern of the spin-coated film showed an isotropic texture and the presence of a secondary peak which corresponded to the 110 planes of the  $\alpha$  phase of the copolymer. The study indicated that the LB-deposited film has greater phase purity in the ferroelectric  $\beta$ -phase. The  $\alpha$ -phase of spin-cast films is paraelectric, which in turn reduces the film polarizability. A P(VDF-TrFE) deposited in an Al substrate was studied by Bystrov et al. with a hysteresis loop of a coercive voltage of about 12 V [105].

Ultrathin films prepared by the LB method are widely used in self-power devices. The loss of materials can be solved by depositing the solution in small drops, providing adequate time for the drops to settle down. Amphiphilic characteristics are not required for the LB method. The orientation of molecules in this method is highly ordered, with high surface pressure assembly, as the fluid sub-phases are completing the adsorption. Studies show that, after annealing, LB films have high crystallinity.

#### 2.4. Composite Prepared from Melt Extrusion Method

In this method, the polymer is melted through a combination of applied heat and friction. It is a solvent-free process. The physical properties of the raw materials are changed by pushing them through the die of the preferred cross-section under elevated controlled temperature and pressure. For fluoropolymer film fabrication, the polymer is loaded into a feed hopper and is gravity-fed into a heated barrel. The polymer is melted gradually and is pushed through the barrel. Through the front end, the molten plastic enters the die. The die gives the final product and is so designed that the molten plastic evenly flows from the cylindrical profile to the profile shape. The extruded film is then cooled to set the film [108,109]. A diagrammatic representation of the melt extrusion method is shown in Figure 13.

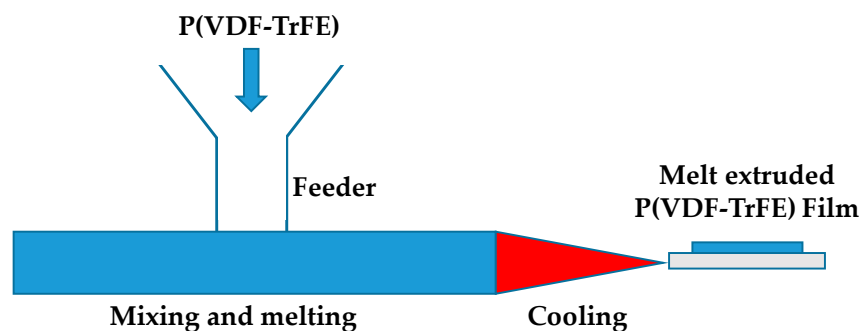


**Figure 13.** Diagrammatic representation of melt extrusion method.

A comparison of the electro-activity behavior of PVDF blended with P(VDF-TrFE) using melt extrusion at 205 °C at different weight ratios of the polymers was conducted by Meng et al. [110]. The blend crystallized to a fine scale of ~40 nm without the appearance of a distinct phase separation. The dielectric value of the blended film increased due to interfacial polarization of the PVDF and P(VDF-TrFE). For blended film  $E_c$  decreases from 83 kVmm<sup>-1</sup> to 32 kVmm<sup>-1</sup> with increasing P(VDF-TrFE) from 10 wt% to 40 wt%. The presence of P(VDF-TrFE) enhanced the  $P_r$  of the blended film to 0.077 cm<sup>-2</sup> with a P(VDF-TrFE) of 40 wt%. Meng et al. fabricated PVDF, P(VDF-TrFE) and a blend of the two (50/50 wt%) using the melt extrusion and hot-pressing method [111]. This blended film showed high values of  $P_r$  due to the highly crystalline  $\beta$  Phase. The dielectric constant of the blended polymer was higher while using the hot press method as well as the extruded film compared to the individual polymers.

The requirements of polymer to withstand shear stress whilst undergoing melt extrusion is the main requirement of the method. The non-requirement of a solvent is the highlight of this method. Even though the method is used in biomedical applications, very few pharmaceutical agents are resistant to the required high temperatures. The pore size of the scaffold produced using the melt extrusion method is not consistent in all directions.

### 2.5. Composite Prepared from Electrospinning Method

The electrospinning method is one of the finest methods to prepare ultrathin fibers. It is basically an electro-hydrodynamic process in which electrification converts a liquid droplet into a jet, which is stretched and elongated to generate fibers. The main component of the setup consists of a syringe, power supply, spinneret, and collective conductor. The main advantage of this method is that the poling and stretching process can be achieved by electric force. Heat treatments for the formation of a desired crystallinity can also be applied accordingly. The type of solvent and molecular weight of the polymer contribute to successful outcomes using the electrospinning method [112–117]. A diagrammatic representation of the electrospinning method is shown in Figure 14.

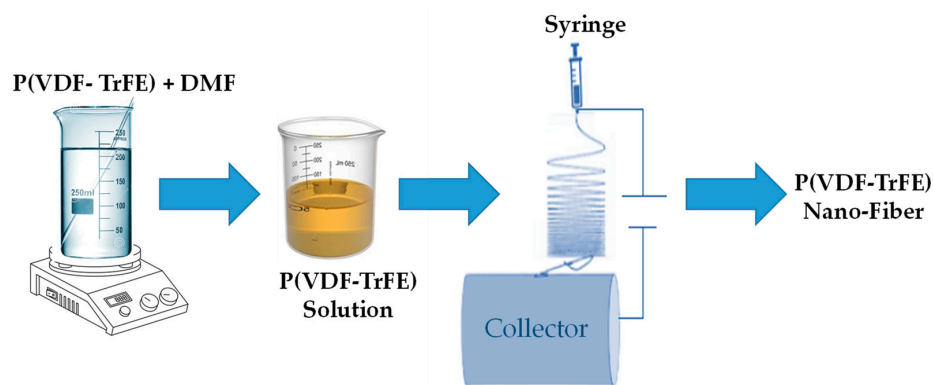


**Figure 14.** Diagrammatic representation of electrospinning method.

Laura et al. fabricated nanogenerators compatible with biomedical applications using the electrospinning method [112]. In this method, the nanofibers were produced with 15 wt% of P(VDF-TrFE) and an MEK solution as solvent. The copolymer was loaded in a syringe with a 20-gauge needle and the collector was placed at a distance of 10 cm. A high voltage power was provided, which was connected to the needle and the collector. The solution pump rate was set at 0.5 to 0.9 mL/h and the voltage applied was 10 kV. The nanogenerator reported  $-0.4$  to  $0.4$  V, at a pressure of 2 and 3 Hz. The piezoelectricity was enhanced with the addition of dH<sub>2</sub>O to the MEK. The polyimide/P(VDF-TrFE) composite triboelectric nanogenerator fabricated by Yeongjum et al. using the electrospinning method reported an output voltage of 364 V and a short-circuit current of 17.2  $\mu$ A [113]. The multi-nozzle drum-system-based nanofiber demonstrated excellent electrical behavior, which can be used in wearable energy harvesters. A comparative study of electrospin speed and the concentration of solution on fabricated electrospun nanofibers was conducted by Pourbafrani et al. [114]. The voltage selected was 20 kV, and the collector distance was 15 cm. The study revealed that, at a constant feed rate, the increase in solution concentration increased the diameter of the fibers. The diameter of the fibers also increased with the feed rate due to the lower stretching capacity of the solution. The study also reported that the piezoelectric measurement of nanofibers with lower diameters generated a very high output voltage. An experimental setup for the fabrication of highly aligned P(VDF-TrFE) by Jiang et al. [115] consisted of microfabricated parallel electrodes on a substrate as a collector. The grounded electrode of the collector was kept open with a gap. P(VDF-TrFE) dissolved in MEK was stirred at 60 °C followed by an ultrasonic bath for 2 min to form a homogeneous solution. A syringe loaded with the copolymer was connected to a high-power supply. The fabricated fiber was highly aligned across the gap, considering the electrostatic force from the grounded electrode. The relative magnitude of the field's horizontal component was increased by increasing the gap between the electrodes, contributing to the alignment of fibers across the gap. Ico et al. [116] reported electrospun P(VDF-TrFE) dissolved in N-N dimethylformamide and acetone after stirring the solution for 1 h. The solution was filled in a syringe of 10 mL with a needle diameter of 250  $\mu$ m. The feed rate was set at 0.5 mL/h. The collector distance was 20 cm from the needle and a positive 0.5 kV was applied to the collector, with negative 14 kV to the syringe. The study revealed that the reduction in dimension resulted in an increase in the electroactive phase content and degree of crystallinity. The reduction in dimension also decreased the Young's modulus. The increase in the piezoelectric component and Young's modulus enhanced the piezoelectric and electrical properties of the nanofiber. Kibra et al. used the electrospinning method for the fabrication of a P(VDF-TrFE)-based sensor for biomedical applications [117]. Nanofiber sensors with different pore diameters, shapes, and sizes were prepared with polydimethylsiloxane. The sensitivity of the sensor was related to the pore diameter; a nanofiber with 250 nm exhibited a sensitivity of 10 VPa<sup>-1</sup>. The pressure sensor fabricated by Arsalon et al. with PEDOT-CNT/rGO composites reported an electrical conductivity of 3916 S/cm for a hybrid nanocomposite and a sensor sensitivity of 67.4 kPa [118].

The electrospinning method consists of a simple setup; however, the mechanism is a complicated one. Although the outcome of the product can be modified by modifying various setup parameters, temperature and humidity are also important factors. Research has pointed out the importance of setup parameters in delivering a fine product, such as the tip-to-collector distance, which is used to determine the diameter of the fiber. A low solution concentration can influence the outcome of electro-spraying, as with a high viscous solution, fiber formation is very rare. Instability during spinning is now widely addressed by researchers, as this can affect the molecular orientation of the fiber. The advantages and disadvantages of the synthesis method are summarized in Table 4.

**Table 4.** Advantages and disadvantages of the synthesis method.

Synthesis Method	Advantages	Disadvantages
Electrospinning method	<ol style="list-style-type: none"> <li>1. Preparation of ultra-thin films with uniformity</li> <li>2. Piezoelectric behaviour of sample without poling and stretching</li> <li>3. Preparation of sample with desired mechanical properties by the fine tuning of heat process</li> <li>4. Higher <math>\beta</math> phase fibre preparation by adjusting electrospinning parameters.</li> </ol>	<ol style="list-style-type: none"> <li>1. Requirement of high electric source</li> <li>2. Use of halogenated and toxic organic solvents</li> </ol>
Spin-coating method	<ol style="list-style-type: none"> <li>1. Fast and easy to operate</li> <li>2. Preparation of thin films</li> <li>3. High reproducibility</li> <li>4. Uniformity of films</li> </ol>	<ol style="list-style-type: none"> <li>1. Porosity and agglomeration</li> <li>2. Crystallization depends on substrate temperature</li> <li>3. Poling of film is generally required for higher piezoelectric nature.</li> <li>4. Annealing is required for <math>\beta</math> Phase.</li> </ol>
Solution casting	<ol style="list-style-type: none"> <li>1. Normally dissolution undergoes at room temperature</li> <li>2. Fabrication of complex shapes</li> <li>3. Dimensional stability</li> <li>4. Lower cost and minimal setup time</li> </ol>	<ol style="list-style-type: none"> <li>1. Application of high temperature and electric filed for production of <math>\beta</math> Phase</li> <li>2. Poling is generally required for higher piezoelectric nature</li> <li>3. Sometimes high temperature is required to improve dissolution.</li> </ol>
Melt Extrusion	<ol style="list-style-type: none"> <li>1. Solvent-free method</li> <li>2. Uniformity</li> </ol>	<ol style="list-style-type: none"> <li>1. Degradation of polymer due to high stress.</li> <li>2. Polymers with high temperature resistance is required.</li> </ol>
LB technique	<ol style="list-style-type: none"> <li>1. Preparation of ultra-thin films</li> <li>2. Deposition of single or multi-layer</li> <li>3. Film has high tunability and polarization switching</li> </ol>	<ol style="list-style-type: none"> <li>1. Complicated and time consuming</li> <li>2. High hydrophobicity</li> <li>3. Low efficiency in reproducibility</li> </ol>

### 3. Application of Piezoelectric P(VDF-TrFE) Composite

The ultrasonic submarine detector fabricated by Langevin was the first application using the piezo-electric effect with quartz crystal during the First World War. As time progressed, piezoelectric composite materials paved the way for the fabrication of a wide range of electronic devices, owing to their individual properties. With properties that include high energy density, low mechanical damping, and easy voltage rectification, P(VDF-TrFE) is a flexible piezoelectric polymer that can be recommended for use in bio-electronic devices, sensors, and in piezoelectric generators. A high piezoelectric charge constant and electromagnetic coupling coefficient are required to obtain maximum power density from a piezoelectric energy harvester. A diagram depicting different synthesis methods and their applications is shown in Figure 15.

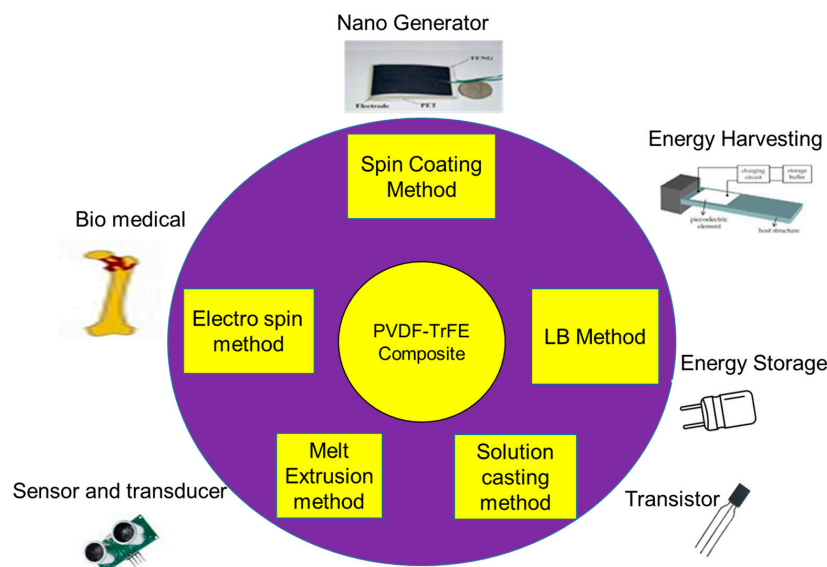


**Figure 15.** Synthesis method of P(VDF-TrFE) film and application.

### 3.1. Energy Harvesting and Nanogenerators

The principle of the conversion of external kinetic energy into electrical energy is used in self-powered electronic devices. Piezoelectric energy harvesters, being highly flexible, compact in size, and having a simple processing technique, have found a firm position among energy scavenging techniques. The excellent piezoelectric and electrostatic properties of P(VDF-TrFE) are a motivating factor for the wide use of polymers in energy harvesting. The performance of nanogenerators prepared by (Na,K)NbO<sub>3</sub> NKN (30–105 nm) embedded in a P(VDF-TrFE) matrix was studied by Kang et al. [119]. Tetradecylphosphonic acid was used for the proper adhesion of nanoparticles with the polymer. The results revealed an increase in the piezoelectric effect of the composite. The output voltage measured was 0.98 V and the output current was ~78 nA, which was increased due to the increase in NKN. Optimization of a PZN/PZT (54 nm) embedded in a P(VDF-TrFE) matrix was conducted by Liu et al. [120] using the electrospinning process for energy harvesting performance. The generator exhibited an output voltage of 3.4 V and a 240 nA output current for a 20% volume of nanoparticles. The piezoelectricity of the composite was found to be five times higher than that of the polymer matrix. The generator exhibited a low resonant frequency (119.56 Hz), a large bandwidth (40.28 Hz), and high-power density (158.33  $\mu\text{W}/\text{cm}^3$ ).

A nanofiber generator based on BZT-BCT and P(VDF-TrFE) of 0-3 composite was proposed by Liu et al. [121] and was prepared by the electrospinning method. BZT-BCT nanoparticles with 10, 20, 30, 40, 50 wt% were mixed into a 40/60 mixture of DMF and acetone. The XRD pattern of the 1-3 composite is shown in Figure 13. The nanofiber mats were prepared by electrospinning with an electric field parameter of 120 V/mm and a spinning speed of 0.2 mL/hr. The generator, with a 40-weight percentage content of BZT-BCT exhibited an admirable output voltage of 13.01 V. The schematic diagram for the experimental setup for characterization of the nanogenerator is represented in Figure 16 and the XRD of the P(VDF-TrFE)/BZT-BCT nanowires is presented in Figure 17.

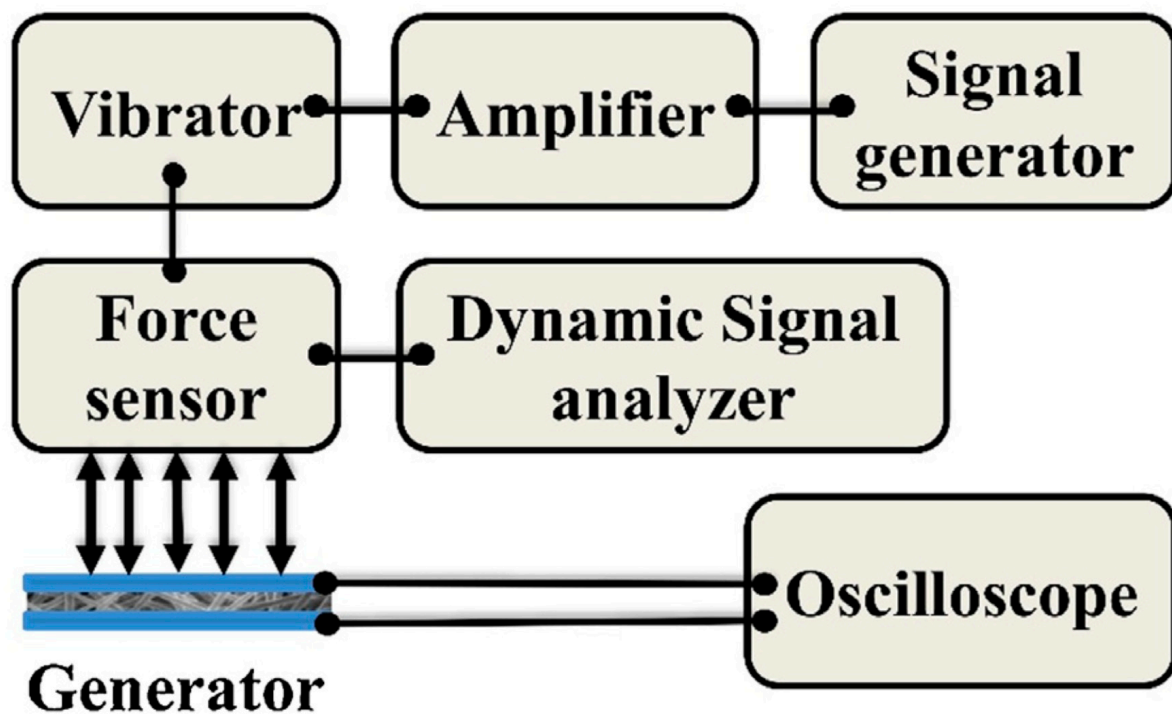


Figure 16. Experimental set up for the characterization of nanogenerator [121].

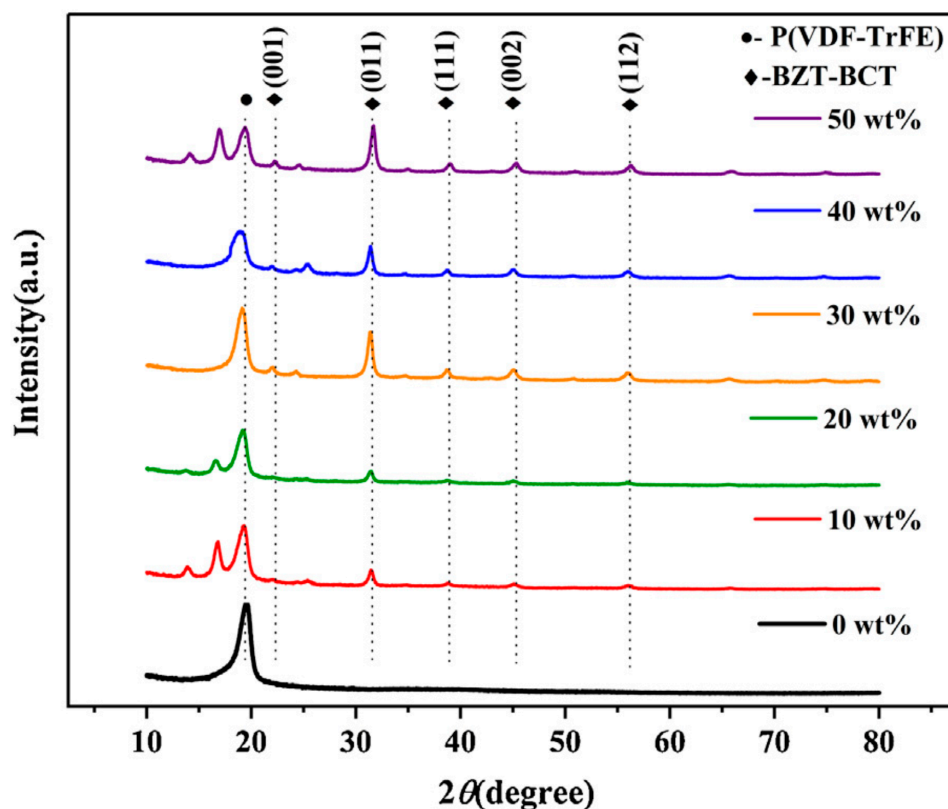


Figure 17. XRD of P(VDF-TrFE)/BZT-BCT nanowires [119].

The flexible triboelectric and piezoelectric hybrid nanogenerator was fabricated by Wang et al. [122]. It consisted of a PDMS/MWCNT membrane and P(VDF-TrFE) nanofibers made by the electrospinning method for wearable and implantable devices and for portable electronic devices. In the open circuit, under a pressure of 5 N, the triboelectric voltage of TPENG was reported to be 25 V and the piezoelectric output peak voltage was 2.5 V. A triboelectric output power and power density of 98.56  $\mu\text{W}$  and 1.98  $\text{mW}/\text{cm}^3$  were observed while connecting to a resistance of 5  $\text{M}\Omega$ . The piezoelectric output power was reported to be 9.747  $\mu\text{W}$ , whereas the power density was 0.689  $\text{mW}/\text{cm}^3$  for a resistance of 30  $\text{M}\Omega$ . A piezoelectric nanogenerator P(VDF-TrFE) polymer was fabricated by Turdakyn et al. using the electrospinning method [123]. The device showed an outstanding peak-to-peak voltage of  $\sim 25$  V under a 3 N applied force and power density of  $\sim 125$   $\text{nW}/\text{cm}^2$  at a 6 N load. The study confirmed the effective use of copolymer in PENG, as the power output received is adequate for its use in low-power electronic devices. Nanogenerators fabricated by Linda et al. used both aligned and random nanofibers fabricated through the electrospinning method [124]. The generated output voltage is proportional to the stress amplitude applied. The nanogenerator, loaded in bending mode, reported a voltage of 270 mV while the compression mode generated a potential of 7 V under an applied force of about 36 N.

Toprak et al. fabricated an energy harvester (cantilever) using multiple piezoelectric polymer layers [125]. A multiple layer of spin coated P(VDF-TrFE) is used to overcome the breakdown voltage of structure layers. A challenge was faced to reduce the resonance frequency to match with frequency range below 250 Hz by decreasing layer thickness. The power output of a film ( $1800 \mu\text{m} \times 2000 \mu\text{m}$ ) was measured at 0.1  $\mu\text{W}$  under an input acceleration of 1.0 g at its resonance frequency of 192.5 Hz. The half-power bandwidth was measured as 2.9 Hz. P(VDF-TrFE)-film-based energy harvesting device on PDMS (polydimethylsiloxane) substrate was demonstrated by Kim et al. [126]. Ti/Ni metal stacks were deposited on the substrate. The device reported a power density of 6.62  $\text{mW}/\text{cm}^3$  for an area of 4  $\text{cm}^2$  with an average voltage of 5.8 V and current of 3.2  $\mu\text{A}$  at 30 Hz and

1.75 g acceleration. The performance of the device was found better than the other flexible energy harvesters. The role of reduced graphene oxide (RGO) as a poling medium in P(VDF-TrFE) was studied by Reheman et al. [127]. The aggregation of RGO in the matrix is due to its large specific surface energy and the existence of an oxygen functional group that optimizes the inter-molecular interaction with the copolymer chain. This results in the formation of a strong bond between the conductor and insulator. The PENG with 0.1% RGO contents reported a maximum open-circuit voltage of 2.4 V and the highest peak of short-circuit current of around 0.8  $\mu\text{A}$  at an applied force of 2 N. The maximum power output of 3.2  $\mu\text{W}$  was exhibited at 1.8 M $\Omega$  load resistance. Yong et al. fabricated an energy harvester with a highly aligned P(VDF-TrFE) fabricated by adjusting the airflow to induce rapid rotation of the drum of the collector [128]. This contributed to the stretching of the fiber and an increase in the  $\beta$  phase. The output voltage produced by the harvester was 116.6 V with an output power of 13.6  $\mu\text{W}$ . Berkay et al. fabricated an energy harvester with P(VDF-TrFE)/polyethylene terephthalate for health-monitoring purposes [129]. A wind test setup was also added to the device. The generator power output was capable of driving a power sensor with a current output of 291.34  $\mu\text{A}$  and a voltage of 937.01 mV; under wind pressure conditions, the reported power output was 272.99  $\mu\text{W}$ .

### 3.2. Sensor Application

Sensors are devices used to sense various types of physical phenomenon from the environment. The electrical signal output generated will be proportional to the applied input. Sometimes this output is used to calibrate the input. The output signal can be transmitted for further processing also. The application of sensors spread wide range from industrial purpose to medical field. A sensor which works on the principle of piezoelectricity is known as a piezoelectric sensor. P(VDF-TrFE), which is both pyroelectric and piezoelectric, is widely used in pressure sensor and temperature sensors. P(VDF-TrFE) sensors are used in health science as they are biocompatible and lightweight. The sensors are also used for the measurement of various physical quantities owing to their wide-frequency response, excellent mechanical properties, cost-effectiveness, and pressure sensitivity.

Three types of sensors were prepared by Zhang et al. [130] using calcium-modified lead titanate (<100 nm) ingrained in a P(VDF-TrFE) matrix to form a 0-3 composite by spin-coating. Configuration 1 consisted of a sensing element deposited on a 380  $\mu\text{m}$  thick Si wafer coated with 1.5  $\mu\text{m}$  thick Si dioxide and a 0.6  $\mu\text{m}$  thick Al electrode. Configuration 2 was similar to 1 with an additional 8  $\mu\text{m}$  thickness. The polyamide layer was deposited between the sensing element and the Si substrate. Configuration 3 had the same structure as configuration 2, with the Si substrate etched away. The specific detectivity showed a maximum value of  $1.3 \times 10^7 \text{ cm Hz}^{1/2}/\text{W}$  for the sensor with configuration 1 and  $2.1 \times 10^7 \text{ cm Hz}^{1/2}/\text{W}$  at about 300 Hz for the sensor with configuration 2. The relative permittivity and pyroelectric coefficient of the prepared polyamides were found to be 14 and 50  $\mu\text{C}/\text{m}^2$ . Pecora et al. fabricated a P(VDF-TrFE) pyroelectric sensor driven by a polysilicon thin film transistor on an ultra-thin polyamide substrate [55]. A Cr-Au/P(VDF-TrFE)/Cr structure was fabricated with Al, forming an insulating region. No electrical breakdown was observed up to 160 V, and a leakage current of  $1 \times 10^{-6}$  A was observed. The pyroelectric sensor capacitor was coupled to a LTPS-TFT (low temperature polycrystalline silicon thin film transistor) in a common source amplifier configuration with an optimized external load resistance of 33 k $\Omega$ . Analysis of the sensor behavior of the IR chopped radiation provided by a laser with a maximum power of 5 mW was conducted. The maximum sensor output obtained was a frequency of 10 Hz and an R bias of 2 M $\Omega$ .

The  $R_{\text{load}}$  was kept constant at an optimized value of 33 K $\Omega$  while the sensor response was collected for three different  $R_{\text{bias}}$ . The peak-to-peak output voltage measured at increasing frequencies (10, 100, 300, 500 and 700 Hz) of the IR laser radiation is given in Figure 18. In the fabrication of a tactical sensor by Hong et al. [56] with a deionized water dissociation treatment on the stainless-steel substrate surface on a P(VDF-TrFE) film by the spin-coating method, a change in remnant polarization with an increase in voltage

was observed. The remnant polarization decreased from  $5.6 \mu\text{C}/\text{cm}^2$  to  $4.61 \mu\text{C}/\text{cm}^2$  for a change of voltage between  $-5 \text{ V}$  and  $-60 \text{ V}$ . A coercive field of  $1000 \text{ KV}/\text{cm}$  was obtained at  $-15 \text{ V}$ . For the substrate treated at  $0 \text{ V}$ , the  $d_{33}$  value reported was approximately  $-10.7 \text{ pC}/\text{N}$  and it reached a minimum of  $-5 \text{ pC}/\text{N}$  at  $-60 \text{ V}$ . Mahdi et al. studied the ferroelectric properties of a thin P(VDF-TrFE) (70/30) film for sensors and actuators at low temperatures by hot plate annealing [57]. The  $\beta$  phase can be crystallized by providing heat treatment to the copolymer. A high remnant polarization ( $P_r$ ) of  $94 \text{ mC}/\text{m}^2$ , pyroelectric constant ( $p$ ) of  $24 \mu\text{C}/\text{m}^2 \text{ K}$ , and a highly crystalline  $\beta$  phase with a rod-like crystal structure were seen at an annealing temperature of  $100 \text{ }^\circ\text{C}$ , slightly above the Curie temperature ( $T_C$ ).

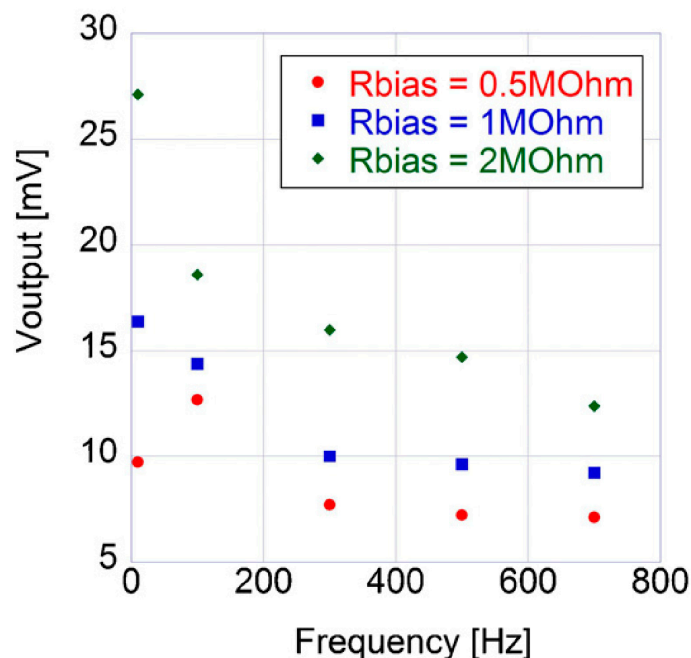


**Figure 18.** Peak-to-peak output voltage measured at increasing frequencies (10, 100, 300, 500 and 700 Hz) of the IR laser radiation [55].

Lie et al. [58] studied the improvement in charge collection of mechanical/thermal sensor fabricated from P(VDF-TrFE) via an electrode interface mechanism. The reported piezoelectric coefficient was  $-86 \text{ pC}/\text{N}$ . The interconnected interface between poly(3,4-ethylene dioxythiophene) doped with a polystyrene sulfonate layer and a copolymer film collected the chargers. Sharma et al. [59] used a spin-coated P(VDF-TrFE) thin film with a high  $\beta$  phase content to fabricate a pressure sensor device using a standard lithography process. The sensor reported a fast recovery time of  $0.17 \text{ S}$  and is applicable for catheter applications. Marchiori et al. developed a sensor for E-skin application. Spin-coated P(VDF-TrFE) was sandwiched between highly stretchable poly (3,4-ethylene dioxythiophene) and a polystyrene sulfonate layer [60]. A sensitivity of approximately  $7 \text{ pF}/^\circ\text{C}$  up to 35% was found, with a pyroelectric peak of  $13 \text{ mV}$  to an IR illumination of  $5 \text{ Mv}$  at  $830 \text{ nm}$ . Wang et al. fabricated an electrospun P(VDF-TrFE)/MXene nanofiber mat [131]. The sensor for 20 wt% of MXene showed output power density of approximately  $3.64 \text{ mW}/\text{m}^2$  under  $20 \text{ N}$  pressure and frequency at  $1 \text{ Hz}$ . The addition of MXene improved the polarization of the copolymer while electrospinning thereby making it highly suitable for health care and environmental study application. Shoubhik et al. fabricated a P(VDF-TrFE)/BaTiO<sub>3</sub> sensor for touch and temperature sensing [132]. The sensor reported a high temperature sensitivity of  $15.34 \text{ mV}/^\circ\text{C}$  with a sensitivity to force/pressure of  $670 \text{ Mv}/\text{N}/7.36 \text{ mV}/\text{N}$ .

### 3.3. Biomedical Application

Nadzrinahamin et al. studied the electron and proton conductive properties of Nafion/P(VDF-TrFE) [133]. The Nafion/P(VDF-TrFE) blends showing an hourglass-type

phase diagram. The P(VDF-TrFE) copolymer exhibited a change from a capacitor to an insulator nature with increasing temperatures. The structural properties of PVDF and P(VDF-TrFE) with natural polymers or starch as additives by compression and annealing were investigated by Simones et al. [134]. It was observed that the polymers do not interact chemically with the additives, whereas the adhesion of starch is better in the copolymer. The density values of the blended films are between 1.5 and 2.0 g/cm<sup>3</sup> and thermal conductivity was in the range of 0.17–0.32 W/mK. Li et al. fabricated electrospun P(VDF-TrFE) scaffolds for bone and neural tissue engineering [135]. The scaffolds produced electrical charges during mechanical deformation and hence provided stimulation to repair the defective bones and damaged nerves. A similar study was conducted by Orkwis et al. [136] for nerve repair applications using electrospun P(VDF-TrFE) scaffolds. The study was conducted with scaffolds with a conduit design that was applicable for peripheral nervous system repair. Adadi et al. designed electrospun P(VDF-TrFE) scaffolds for cardiac tissue engineering [137]. The P(VDF-TrFE) scaffolds function as a sensor, which in turn supports cardiac myocytes culture and promotes the assembly of cardiac tissues, generating contractions.

### 3.4. Transducer and Resonator

P(VDF-TrFE) is the most promising polymer for the fabrication of transducers and resonators. The copolymer is widely used in microelectromechanical systems (MEMS), especially transducers and resonators, due to its high piezoelectric and electromechanical nature. The large electromechanical coupling factor is due to the high crystallinity and remnant polarization of the copolymer. FBAR (thin-film-based acoustic resonators) are used in radiofrequency filters and oscillators. The application of a P(VDF-TrFE) film in ultrasonic transducers was studied by Hiroji et al. [138]. For usage as a transducer, a P(VDF-TrFE) thin film was coated with a backing electrode using the spin-coating method. After heat treatment and the deposition of a suitable electrode, poling was conducted. The resonance curve indicated that piezoelectric activity persisted at a low temperature. The elastic constant and mechanical quality factor increased with decreases in temperature, whereas the dielectric constant and mechanical loss factor both decreased with decreasing temperatures. The temperature-independent  $k_t$  (electro-mechanical coupling factor) and its thermal stability up to a Curie temperature confirmed that the piezoelectricity of the copolymer originated from the ferroelectric nature of the crystal, the polarization of which was oriented as normal to the film surface. The value of  $kt$  for the copolymer film was independent of temperature in the ranged from 120–350 K to 120–370 K. The film material is highly effective against thermal strain and the acoustic impedance is less than that of other organic piezoelectric materials and could be used as an ultrasonic transducer in acoustic applications for solids and liquids at low temperatures. The methodical optimization of various processing conditions for P(VDF-TrFE) thin films through integrated transducers in a MEMS resonator was studied by Pierre et al. [139]. The samples were annealed at 140 °C after spin-coating. The results of the poling showed that the  $d_{33}$  value depends only on the field applied but not on the duration of poling, whereas the optimal annealing temperature must be between the Curie temperature and melting temperature. The paraelectric phase allowed for better chain mobility which in turn led to high crystallinity. High mobility of the copolymer chain occurs during annealing and only a few minutes of annealing were required to obtain the piezoelectric effect of the sample. The study showed that the ideal poling electric field at room temperature was 100 V μm<sup>-1</sup>, beyond which there was no improvement in the piezoelectric property. Kaneko et al. studied the development of a bulk acoustic resonator [140]. A PVDF-TrFE/SiO<sub>2</sub> composite FBAR (film bulk acoustic wave resonator) was designed, simulated, and developed. After poling, the thickness expansion mode was observed at 387.4 MHz. The impedance ratio was 4.95–10.3 dB, the electromechanical coupling factor was 6.05–7.95% and the mechanical quality factor was 20–33 and was also radius-dependent. The increase in the radius of the device increased the impedance ratio, coupling coefficient ( $k_2$ ), mechanical quality factor ( $Q_m$ ), and figure of merit of the device. The maximum  $Q_m$  was 33 for an 80 μm radius of the device and the

residual film stress of P(VDF-TrFE) was reported to be 34.8 MPa for tensile mean stress and −79.7 kPa for gradient stress.

Takahashi et al. investigated the properties and characteristics of P(VDF/TrFE) transducers in the MHz-range ultrasound in air [141]. Piezoelectric polymer transducers with high operating frequencies at 4,6 and 10 MHz were fabricated using the solution casting method. A 57 dB transducer operating at 6 MHz was fabricated on the backing plate/electrode; at 6 MHz a  $k_t$  value of 0.27 was obtained.

Low-voltage-operated polymer transistors with a high-capacitance P(VDF-TrFE)/(PVDF) film as a gate dielectric layer were fabricated by Jung et al. [142]. The surface morphologies and crystallinity of the film changed when PVDF was included. The pure P(VDF-TrFE) film crystal had long rod-like features. The diameter of the rigid rod-like crystals decreased with the addition of PVDF. The root mean square roughness of the P(VDF-TrFE)/(PVDF) (60:40) and (20:80) were 5.93 nm and 6.7 nm, respectively. The study of P-E characterization of the MFM capacitor showed a decrease in remnant polarization by increasing the concentration of PVDF, as shown in Table 5, and the comparative study of the XRD patterns of different compositions of PVDF/PDF-TrFE is shown in Figure 19. Properties of the P(VDF-TrFE)/PVDF film and F8T2 top-gate transistors with a P(VDF-TrFE)/PVDF gate dielectric layer are given in Table 5.

**Table 5.** Properties of P(VDF-TrFE)/PVDF film and F8T2 top-gate transistors with P(VDF-TrFE)/PVDF gate dielectric layer [142].

PVDF Concentration (%)	Roughness (nm)	E	Remnant Polarization (mC/cm <sup>2</sup> )
0	5.93	8.6	8.4
20	5.36	9	5.5
40	4.11	9.4	4.3
80	6.70	10.2	0.2

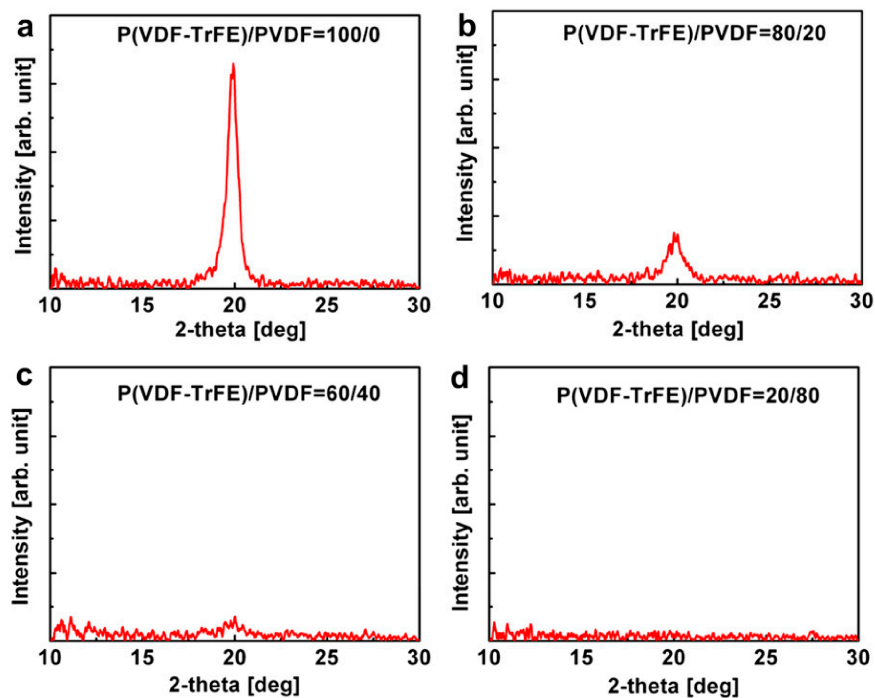


**Figure 19.** X-ray diffraction pattern of (a) bare P(VDF-TrFE) film and P(VDF-TrFE)/PVDF films: (b) 80/20, (c) 60/40 and (d) 20:80 blends [142].

The various synthesis processes of composite films and their outcomes are presented in Table 6.

**Table 6.** Synthesis and Outcome of P(VDF-TrFE) and P(VDF-TrFE) composites.

Sr No	Sample Prepared	Method of Preparation	Dielectric Out come	Ferroelectric Outcome	Piezoelectric Outcome	Electrical Outcome	Reference
1	Fe(0.05) doped ZnO/P(VDF-TrFE)	Solvent casting	21.03 at 1 kHz	Pr: 0.125 $\mu\text{C}/\text{cm}^2$	-	Output voltage ~ 7 V	R Sahoo et al. [143]
2	Ca doped ZnO/P(VDF-TrFE)	Solvent casting	15.3	Pr: 0.125 $\mu\text{C}/\text{cm}^2$ $E_c$ 41 MV/m	-	Output voltage 3 V	R Sahoo et al. [144]
3	CO/P(VDF-TrFE)/PDMS/Nylon/Ag	Electro Spinning	-	-	$d_{33}$ : $-20 \text{ pmV}^{-1}$	3.9 V (10 pieces of C-PEG) 9.5 V (20 pieces of C-PEG)	J H Kim et al. [145]
4	P(VDF-TrFE)	Solution casting	12 (VDF:TrFE-71:29) 11 (VDF:TrFE-72.2:27.8)	Pr: 5.7 $\mu\text{C}/\text{cm}^2$ $E_c$ 56.8 MV/m(VDF:TrFE-71:29) Pr: 6.5 $\mu\text{C}/\text{cm}^2$ $E_c$ 54.7 MV/m(VDF:TrFE-71:29)	$d_{33}$ : $-58 \text{ p C/N}$ (VDF:TrFE-72.2:27.8)	-	A Aliane et al. [146]
5	P(VDF-TrFE)/NiFe <sub>2</sub> O <sub>4</sub>	Spin Coating	-	-	$d_{33}$ : 32 p C/N(NF 1 wt%) 26 p C/N(NF 0.5 wt%)	Output Voltage—1.4 V, Power density—0.05 Mw/cm <sup>3</sup>	Sujoy Kumar et al. [147]
6	P(VDF-TrFE)	Solution Casting	11.9	Pr: 11.4 $\mu\text{C}/\text{cm}^2$	$d_{33}$ :25 p C/N	-	Q.Q Sun et al. [148]
7	P(VDF-TrFE)/FeCoSiB	Solution casting	-	-	$d_{33}$ : 34.87 p C/N	ME voltage-111 V/cm.Oe	Dandan Wen et al. [149]
8	P(VDF-TrFE)/BiFeO <sub>3</sub> -NaNbO <sub>3</sub>	Spin Coating	-	$P_S$ : 8 $\mu\text{C}/\text{cm}^2$ for 5% vol % of BiFeO <sub>3</sub> -NaNbO <sub>3</sub>	$d_{33}$ : 34 p C/N for 5 vol % of BiFeO <sub>3</sub> -NaNbO <sub>3</sub> $d_{33}$ : 38 p C/N for 10 vol % of BiFeO <sub>3</sub> -NaNbO <sub>3</sub>	--	R P Ummer et al. [150]
9	P(VDF-TrFE)/Carbon Nanotubes	Solution Casting	-	-	$d_{33}$ 26.4 $\pm$ 1.3 pC/N	Voltage—2.7 V	Jia Wun Li et al. [151]
10	P(VDF-TrFE)/Polysterene	Solution casting	18.8 at 10 <sup>3</sup> Hz for 10 wt% of CTAB modified PS.	-	-	Short circuit current density 47.45 mA, Peak power density: 7.88 W/m <sup>2</sup>	Liqin Yao et al. [152]
11	P(VDF-TrFE)	Electro Spinning	-	-	$d_{31}$ 22.88 pC/N	Voltage 1.7 V Current 41.5 nA	Aochen Wang et al. [153]
12	P(VDF-TrFE)	Spin Coating	-	2Pr: 5.55 $\mu\text{C}/\text{cm}^2$	-	Open circuit output Voltage—4.02 V	Yi Pei Jang et al. [154]
13	P(VDF-TrFE), PEDOT:PSS	Electro Spinning	-	-	$d_{33\text{eff}}$ ~ 31.5 $\text{pmV}^{-1}$ (no core sample) $d_{33\text{eff}}$ ~ 58.3 $\text{pmV}^{-1}$ (0.65:1) sample	Output voltage 8.76 V, Current 547 nA	Ju Han et al. [155]

Table 6. Cont.

Sr No	Sample Prepared	Method of Preparation	Dielectric Out come	Ferroelectric Outcome	Piezoelectric Outcome	Electrical Outcome	Reference
14	P(VDF-TrFE)/Neodymium/Cobalt	Spin Coating	30–40		$d_{33} 26.4 \pm 1.3 \text{ pC/N}$	Conductivity $3 \times 10^6 - 1 \times 10^9$	N Hernandez et al. [156]
15	P(VDF-TrFE)	Spin Coating	-	Pr: $6.1 \mu\text{C}/\text{cm}^2$ $E_c 74.9 \text{ V}/\mu\text{m}$	-	Output Power 35.1 pW, Power Output Density—97.5 $\text{pW}/\text{mm}^2$	Alperen Toprak et al. [157]
16	P(VDF-TrFE)	Spin Coating	-	$E_c 55 \text{ V}/\mu\text{w}$	$d_{33} 23.9 \text{ pm/V}$	-	Alperen Toprak et al. [158]
17	P(VDF-TrFE)	Solution Casting	-	-	$d_{33} - 28 \text{ pC/N}$	Output Voltage 8.7 V	X Hu et al. [159]
18	P(VDF-TrFE)	Spin Coating	-	Pr: $5.6 \mu\text{C}/\text{cm}^2$ at $-5 \text{ V}$ Pr: $4.61 \mu\text{C}/\text{cm}^2$ at $-60 \text{ V}$ $E_c 1000 \text{ kV}/\text{cm}$ at $-15 \text{ V}$	$d_{33} - 10.7 \text{ pC/N}$ at $0 \text{ V}$ $d_{33} - 5 \text{ pC/N}$ at $-60 \text{ V}$	-	H J Tseng et al. [56]
19	P(VDF-TrFE)	Solution casting			$d_{33} 10.7 \text{ pC/N}$	Output Voltage 8.7 V	G Ahn et al. [160]
20	P(VDF-TrFE)	Spin Casting		Pr: $4.7 \mu\text{C}/\text{cm}^2$ $E_c 53 \text{ V}\mu\text{m}^{-1}$	$d_{33} - 29.8 \text{ pmV}^{-1}$		D Dishan et al. [161]

#### 4. Conclusions and Future Scope

This review mainly concentrates on the different processing methods of P(VDF-TrFE) composites and their applications. P(VDF-TrFE)-based polymer composites are widely used in sensors, generators, transducers, and biomedical applications. Studies have widely investigated the energy harvesting applications of the polymer composite with increases in piezoelectricity, output current, and voltage achieved with the addition of fillers. High flexibility and power density are the two main highlights of piezoelectric vibrational harvesters. A change in relatively low pressure can be detected by piezoelectric sensors, as their sensitivity is determined mostly by their piezoelectricity and permittivity. They are most frequently used in tissue engineering applications.

The spin-coating technique is one of the simplest and easiest cost-effective routes for uniform polymer composite film fabrication, which makes it ideal for research and other electronic applications. Variations in annealing temperatures play a significant role in the crystallization of the film. Studies have emphasized that the lower spinning speed of the system favors the formation of a ferroelectric phase. The solution casting method is widely used for the fabrication of films with complex shapes. Here, the properties of the composite depend on the solvent used in the method. P(VDF-TrFE)-based film fabricated by the LB method has provided many new opportunities in microelectronics. Single and multi-molecular films of desired thicknesses can be formed by the Langmuir–Blodgett method, with a polarization switching mechanism. The electrospinning method is mainly used for the fabrication of piezoelectric nanogenerators because of the large  $\beta$  phase content. Fillers improve the crystallinity,  $\beta$  phase, and grain growth of the polymer composite by annealing it at temperatures between the Curie temperature and melting point. Stretching and polarization of the polymer composite are among the prominent processes used to enhance the piezoelectric effect.

The fabrication process plays a vital role in the final properties of PVDF-TrFE composites. The excellent ferroelectric and piezoelectric properties of the composites play a significant role in energy harvesting and in the medical field. Although widespread studies are in progress for the enhancement of their physical and chemical properties using different fabrication methods, the electrospinning method has emerged as the most promising method for piezoelectric devices. Despite advances, the choice of additives and the amounts used are significant for the enhancement of desired properties. Future research may lead to the commercial production of devices, mainly in the medical field and for self-charging technologies.

**Author Contributions:** Conceptualization, S.B. and S.P.; methodology, software, validation, L.P.P.S. and B.S.; formal analysis, investigation, resources, data curation, S.R., L.P.P.S. and B.S.; writing—original draft preparation, L.P.P.S. and B.S.; writing—review and editing, S.R., S.B. and S.P.; supervision, S.B. and S.P.; project administration, S.B. and S.P.; funding acquisition, S.B. and S.P. All authors have read and agreed to the published version of the manuscript.

**Funding:** This research received no external funding.

**Data Availability Statement:** The data presented in this study are available on request from the corresponding author.

**Conflicts of Interest:** The authors declare no conflict of interest.

#### References

1. Habib, M.; Lantgios, I. A review of ceramic, polymer and composite piezoelectric Materials. *J. Phys. D Appl. Phys.* **2022**, *55*, 423002. [[CrossRef](#)]
2. Santucci, S.; Esposito, V. Electrostrictive Ceramic and their application. In *Encyclopedia of Materials: Technical Ceramics and Glasses*; Pomeroy, M., Ed.; Elsevier: Amsterdam, The Netherlands, 2021; Volume 3, pp. 369–374.
3. Lipsa, L.; Rajput, S.; Parida, S.; Ghosh, S.P.; Verma, S.K.; Gupta, S. Influence of Hot-press Temperature on  $\beta$ -phase Formation and Electrical Properties of Solvent Casted PVDF-HFP Co-Polymer Films Prepared from Two Different Solvents: A Comparison Study. *Macromol. Chem. Phys.* **2023**, *224*, 2300204. [[CrossRef](#)]

4. Abbasipour, M.; Khajavi, R. A comprehensive review on piezoelectric polymeric and ceramic nano generators. *Adv. Eng. Mater.* **2022**, *24*, 2101312. [[CrossRef](#)]
5. Muduli, S.P.; Parida, S.; Behura, S.K.; Rajput, S.; Rout, S.K.; Sareen, S. Synergistic effect of graphene on dielectric and piezoelectric characteristic of PVDF-(BZT-BCT) composite for energy harvesting applications. *Polym. Adv. Tech.* **2022**, *33*, 3628–3642. [[CrossRef](#)]
6. Eltouby, P.; Shyha, I.; Li, C.; Khaliq, J. Factors affecting the piezoelectric performance of ceramic-polymer composites: A comprehensive Review. *Ceram. Int.* **2021**, *47*, 17813–17825. [[CrossRef](#)]
7. Rajput, S.; Parida, S.; Sharma, A.; Sonika. *Dielectric Materials for Energy Storage and Energy Harvesting Devices*; River Publishers: Aalborg, Denmark, 2023; Available online: <https://ieeexplore.ieee.org/book/10177830> (accessed on 1 October 2023).
8. Zielinski, T.G. Fundamentals of multiphysics modeling of piezo-poro-elastic structures. *Arch. Mech.* **2010**, *62*, 343–378.
9. Stefanescu, D.M. *Handbook of Force Transducer Principles and Components*; Springerlar: Berlin, Germany, 2011.
10. Uchino, K. (Ed.) The Development of piezoelectric materials and the new perceptive. In *Advanced Piezoelectric Materials*, 2nd ed.; Woodhead Publishing: Swaston, UK, 2017; pp. 1–92.
11. Rajput, S.; Sharma, A.; Jatily, V.; Ram, M. *Recent Advances in Energy Harvesting Technologies*; River Publishers: Aalborg, Denmark, 2023; ISBN 978-8770228459. e-ISBN 978-8770228800. [[CrossRef](#)]
12. Lewiner, J. Paul Langevin and the birth of ultrasonics. *Jpn. J. Appl. Phys.* **1991**, *30*, 5. [[CrossRef](#)]
13. Camargo-Chavez, J.E.; Arceo-Diaz, S.; Bricio-Barrios, E.E.; Chavez-Valdez, R.E. Piezoelectric mathematical modeling, technological feasibility in the generation and storage of electric charges. *Phys. Conf. Ser.* **2022**, *2159*, 012009. [[CrossRef](#)]
14. Khanbareh, H.; Rasheed, A.; Khaliq, J. 13—Piezoelectric composites. In *Organic Ferroelectric Material and Application*; Asadi, K., Ed.; Woodhead Publishing: Swaston, UK, 2022; pp. 457–475.
15. Mishra, S.; Unnikrishnan, L.; Nayak, S.K.; Mohanty, S. Advances in piezoelectric polymer composites for energy harvesting applications. A systematic Review. *Macromol. Mater. Eng.* **2019**, *304*, 1800463. [[CrossRef](#)]
16. Kawai, H. The Piezoelectricity of PVDF. *Jpn. J. Appl. Phys.* **1969**, *8*, 975. [[CrossRef](#)]
17. Xin, Y.; Zhu, J.; Sun, H.; Xu, Y.; Liu, T.; Qian, C. A brief review on piezoelectric PVDF nanofibers prepared by electrospinning. *Ferroelectrics* **2018**, *526*, 140–151. [[CrossRef](#)]
18. Ueberschlag, P. PVDF piezoelectric polymer. *Sens. Rev.* **2001**, *21*, 118–125. [[CrossRef](#)]
19. Kabir, E.; Khatun, M.; Nasrin, L.; Raihan, M.J.; Rahman, M. Pure  $\beta$ -phase formation in polyvinylidene fluoride (PVDF)-carbon nanotube composites. *J. Phys. D Appl. Phys.* **2017**, *50*, 163002. [[CrossRef](#)]
20. Sonika; Verma, S.K.; Samanta, S.; Srivastava, A.K.; Biswas, S.; Alsharabi, R.M.; Rajput, S. Conducting Polymer Nanocomposite for Energy Storage and Energy Harvesting Systems. *Adv. Mater. Sci. Eng.* **2022**, *2022*, 2266899. [[CrossRef](#)]
21. Dallaev, R.; Pisarenko, T.; Sobola, D.; Orudzhev, F. Brief Review of PVDF properties and application. *Polymers* **2022**, *14*, 4793. [[CrossRef](#)]
22. Wua, L.; Jing, M.; Liua, Y.; Ning, H.; Liu, X.; Liu, S.; Lina, L.; Hu, N.; Liu, L. Power generation by PVDF-TrFE/graphene nanocomposite films. *Compos. Part B Eng.* **2019**, *164*, 703–709. [[CrossRef](#)]
23. Mokhtari, F.; Latifi, M.; Shamshirsaz, M. Electrospinning/electrospray of polyvinylidene fluoride (PVDF): Piezoelectric nanofibers. *J. Text. Inst.* **2016**, *107*, 1037–1055. [[CrossRef](#)]
24. Salimi, A.; Yousefi, A.A. FTIR studies of  $\beta$ -phase crystal formation in stretched PVDF films. *Polym. Test* **2003**, *22*, 699–704. [[CrossRef](#)]
25. Correia, H.M.G.; Ramos, M.M.D. Quantum modelling of poly (vinylidene fluoride). *Comput. Mater. Sci.* **2005**, *33*, 224–229. [[CrossRef](#)]
26. Martins, P.; Lopes, A.C.; Lanceros-Mendez, S. Electroactive phases of poly(vinylidene fluoride): Determination, processing and applications. *Prog. Polym. Sci.* **2014**, *39*, 683–706. [[CrossRef](#)]
27. Kim, Y.; Xie, Y.; Wen, X.; Wang, S.; Kim, S.J.; Song, H.; Wang, Z. Highly porous piezoelectric PVDF membrane as effective lithium ion transfer channels for enhanced self-charging power cell. *Nano Energy* **2014**, *14*, 77–86. [[CrossRef](#)]
28. Broadhurst, M.G.; Davis, G.T. Physical basis for piezoelectricity in PVDF. *Ferroelectrics* **1984**, *60*, 3–13. [[CrossRef](#)]
29. Cardoso, V.F.; Minas, G.; Costa, C.M.; Tavares, C.J.; Lanceros-Mendez, S. Micro and nano films of poly (vinylidene fluoride) with controlled thickness, morphology and electroactive crystalline phase for sensor and actuator applications. *Smart Mater. Struct.* **2021**, *20*, 087002. [[CrossRef](#)]
30. Muduli, S.; Parida, S.; Rout, S.; Rajput, S.; Kar, M. Effect of hot press temperature on-phase, dielectric and ferroelectric properties of solvent casted Poly(vinylidene fluoride) films. *Mater. Res. Exp.* **2019**, *6*, 095306. [[CrossRef](#)]
31. Pramod, K.; Gangineni, R.B. Influence of solvent evaporation rate on crystallization of poly (vinylidene fluoride) thin films. *Bull. Mater. Sci.* **2015**, *38*, 1093–1098. [[CrossRef](#)]
32. Naik, R.; Rao, T.S. Preparation and characterization of flexible PVDF based polymer film for energy harvesting applications. *Mater. Today Proc.* **2019**, *18*, 5107–5113. [[CrossRef](#)]
33. Gregorio, R., Jr.; Capitão, R.C. Morphology and phase transition of high melt temperature crystallized poly (vinylidene fluoride). *J. Mater. Sci.* **2000**, *35*, 299–306. [[CrossRef](#)]
34. Gregorio, R., Jr.; Ueno, E.M. Effect of crystalline phase, orientation and temperature on the dielectric properties of poly (vinylidene fluoride) (PVDF). *J. Mater. Sci.* **1999**, *34*, 4489–4500. [[CrossRef](#)]
35. Furukawa, T. Ferroelectric properties of vinylidene fluoride copolymers. *Phase Transit.* **1989**, *18*, 143–211. [[CrossRef](#)]

36. Nalwa, H.S. Crystal Structure and Phase Transition of PVDF and Related Copolymers. In *Ferroelectric Polymers Chemistry, Physics and Applications*, 1st ed.; Nalwa, H.S., Ed.; Marcel Dekker, Inc.: New York, NY, USA, 1995; pp. 63–181.
37. Reynolds, N.M.; Kim, K.J.; Chang, C.; Hsu, S.L. Spectroscopic analysis of the electric field induced structural changes in vinylidene fluoride/trifluoroethylene copolymers. *Macromolecules* **1989**, *22*, 1092–1100. [[CrossRef](#)]
38. Kobayashi, M.; Tashiro, K.; Tadokoro, H. Molecular vibrations of three crystal forms of poly(vinylidene fluoride). *Macromolecules* **1975**, *8*, 158–171. [[CrossRef](#)]
39. Chisca, S.; Sava, I.; Musteata, V.; Bruma, M. Dielectric and conduction properties of polyimide films. In Proceedings of the IEEE International Semiconductor Conference, Sinaia, Romania, 17–19 October 2011; IEEE: Piscataway, NJ, USA, 2011.
40. Kuang, D.; Li, R.; Pei, J. Polyamide 11/Poly(vinylidene fluoride)/Vinyl Acetate-Maleic Anhydride Copolymer as Novel Blends Flexible Materials for Capacitors. *Polymer* **2014**, *6*, 2146–2156. [[CrossRef](#)]
41. Zhao, C.; Hong, Y.; Chu, X.; Dong, Y.; Hu, Z.; Sun, X.; Yan, S. Enhanced ferroelectric properties of P(VDF-TrFE) thin film on single layer graphene simply adjusted by crystallization condition. *Mater. Today Energy* **2021**, *20*, 100678. [[CrossRef](#)]
42. Wu, T.; Jin, H.; Dong, S.; Xuan, W.; Xu, H.; Lu, L.; Fang, Z.; Huang, S.; Tao, X.; Shi, L.; et al. A Flexible Film Bulk Acoustic Resonator Based on  $\beta$ -Phase Polyvinylidene Fluoride Polymer. *Sensors* **2020**, *20*, 1346. [[CrossRef](#)]
43. Veved, A.; Ejuh, G.W.; Djongyang, N. Review of emerging materials for PVDF based energy harvesting. *Energy Rep.* **2022**, *8*, 12853–12870. [[CrossRef](#)]
44. Zhang, W.; Zaarour, B.; Zhu, L.; Huang, C.; Xu, B.; Jin, X. A comparative study of electrospun polyvinylidene fluoride and poly(vinylidene fluoride-co-fluoroethylene) fiber webs: Mechanical properties, crystallinity and piezoelectric properties. *J. Eng. Fibers Fabr.* **2020**, *15*, 1–8.
45. Wu, L.; Jin, Z.; Liu, Y.; Ning, H.; Liu, X.; Alamusi, H.; Hu, N. Recent advances in the preparation of PVDF-based piezoelectric material. *Nanotechnol. Rev.* **2022**, *11*, 0082. [[CrossRef](#)]
46. Wang, J.L.; Meng, X.J.; Chu, J.H. *New Properties and Applications of Polyvinylidene Based Ferroelectric Polymer*; Barranco, A.P., Ed.; Intech Open: London, UK, 2015; pp. 151–171.
47. Shafee, E.E.; Behery, S.M. Preparation, characterization and properties of novel 0–3 ferroelectric composites of Ba<sub>0.95</sub>Ca<sub>0.05</sub>Ti<sub>0.8</sub>Zr<sub>0.2</sub>O<sub>3</sub>-poly(vinylidene fluoride-trifluoroethylene). *Mater. Chem. Phys.* **2012**, *132*, 740–746. [[CrossRef](#)]
48. Sheng, Y.; Zhang, X.; Ye, H.; Liang, L.; Xu, L.; Wu, H. Improved energy density in core-shell poly(dopamine) coated barium titanate/poly(vinylidene fluoride-co-trifluoroethylene) nanocomposite with interfacial polarization. *Colloids Surf. B* **2020**, *585*, 124091. [[CrossRef](#)]
49. Nunes-Pereira, J.; Martins, P.; Cardoso, V.F.; Costa, C.M.; Lanceros-Mendez, S. A green solvent strategy for the development of piezoelectric poly(vinylidene fluoride-trifluoroethylene) films for sensors and actuators application. *Mater. Des.* **2016**, *104*, 183–189. [[CrossRef](#)]
50. Vacche, S.D.; Damjanovic, D.; Michaud, V.; Leterrier, Y. Interface-Dominated Time-Dependent Behavior of Poled Poly (Vinylidene Fluoride-Trifluoroethylene)/Barium Titanate Composites. *Materials* **2020**, *13*, 225. [[CrossRef](#)]
51. Wang, J.; Li, Z.; Yan, Y.; Wang, X.; Zhang, Z. Improving Ferro- and Piezo-Electric Properties of Hydrogenized Poly(vinylidene fluoride-trifluoroethylene) Films by Annealing at Elevated Temperatures. *Chin. J. Polym. Sci.* **2016**, *34*, 649–658. [[CrossRef](#)]
52. Qian, J.; Jiang, S.; Wang, Q.; Zheng, S.; Guo, S.; Yi, C.; Wang, J.; Wang, X.; Tsukagoshi, K.; Shi, Y.; et al. Unveiling the piezoelectric nature of polar  $\alpha$ -phase P(VDF-TrFE) at quasi-two-dimensional limit. *Sci. Rep.* **2018**, *8*, 532. [[CrossRef](#)]
53. Poulsen, M.; Sorokin, A.V.; Adenwalla, S.; Ducharme, S.; Fridkin, V.M. Effects of an external electric field on the ferroelectric-paraelectric phase transition in polyvinylidene fluoride-trifluoroethylene copolymer Langmuir-Blodgett films. *J. Appl. Phys.* **2008**, *103*, 034116. [[CrossRef](#)]
54. Lindemann, W.R.; Philip, R.L.; Chan, D.W.W.; Ayers, C.T.; Perez, E.M.; Beckman, C.P.; Strzalka, J.; Chaudhary, S.; Vaknin, D. Oriented Polyvinylidene Fluoride-Trifluoroethylene films by Langmuir-Blodgett deposition: A synchrotron X ray diffraction study. *Phys. Chem. Chem. Phys.* **2015**, *17*, 29335–29339. [[CrossRef](#)] [[PubMed](#)]
55. Pecora, A.; Maiolo, L.; Maita, F.; Minotti, A. Flexible PVDF-TrFE pyroelectric sensor driven by polysilicon thin film transistor fabricated on ultra-thin polyimide substrate. *Sens. Actuators Rep.* **2012**, *185*, 39–43. [[CrossRef](#)]
56. Taseng, H.J.; Tian, W.C.; Wu, W.C. P(VDF-TrFE) Polymer-Based Thin Films Deposited on Stainless Steel Substrates Treated Using Water Dissociation for Flexible Tactile Sensor development. *Sensors* **2013**, *13*, 14777–14796. [[CrossRef](#)] [[PubMed](#)]
57. Mahd, R.I.; Gan, W.C.; Majid, W.H.A. Hot Plate Annealing at a Low Temperature of a Thin Ferroelectric P(VDF-TrFE) Film with an Improved Crystalline Structure for Sensors and Actuators. *Sensors* **2014**, *14*, 19115–19127. [[CrossRef](#)]
58. Li, B.; Cai, C.; Liu, Y.; Wang, F.; Li, Q.; Zhang, P.; Deng, B.; Hou, P.; Liu, W. Ultrasensitive mechanical/thermal response of a PVDF-TrFE sensor with a tailored network inter connection interface. *Nat. Commun.* **2023**, *14*, 4000. [[CrossRef](#)] [[PubMed](#)]
59. Sharma, T.; Je, S.; Gill, B.; Zhang, J.X.J. Patterning piezoelectric response of PVDF-TrFE based pressure sensor for catheter application. *Sens. Actuators A* **2012**, *177*, 87–92. [[CrossRef](#)]
60. Marchiori, B.; Regal, S.; Arango, Y.; Delattre, R.; Blayac, S.; Ramuz, M. PVDF-TrFE based stretchable contact and non-contact temperature sensor for E-skin application. *Sensors* **2020**, *20*, 623. [[CrossRef](#)]
61. Baur, C.; Zhou, Y.; Sipes, J.; Priya, S.; Voit, W. Organic, Flexible, Polymer Composites for High-Temperature Piezoelectric Applications. *Energy Harvest. Syst.* **2014**, *1*, 167–177. [[CrossRef](#)]
62. Nalwa, H.S.; Watanabe, T.; Kakuta, A.; Mukoh, A.; Miyata, S. Second-order nonlinear optical properties of an aromatic polyurea exhibiting optical transparency down to 300 nm. *Appl. Phys. Lett.* **1993**, *62*, 3223–3225.

63. Yoo, S.; Kim, D.G.; Ha, T.; Won, J.C.; Jang, K.S.; Kim, Y.H. Solution-Processable, Thin, and High- $\kappa$  Dielectric Polyurea Gate Insulator with Strong Hydrogen Bonding for Low-Voltage Organic Thin-Film Transistors. *Appl. Mater. Interfaces* **2018**, *10*, 32462–32470. [CrossRef] [PubMed]
64. Fitzgerald, E.R.; Miller, R.F. Dielectric properties of the system polyvinyl Chloride-Dimethylthianthrene. *J. Colloid. Sci.* **1953**, *8*, 148–169. [CrossRef]
65. Kalimuldina, G.; Turdakyn, N.; Abay, I.; Medeubayev, A.; Nurpeissova, A.; Adair, D.; Bakenov, Z. A Review of Piezoelectric PVDF Film by Electro spinning and its Applications. *Sensors* **2020**, *20*, 5214. [CrossRef] [PubMed]
66. Padurariu, L.; Brunengo, E.; Canu, G.; Curecheriu, L.P.; Conzatti, L.; Buscaglia, M.T.; Stagnaro, P.; Mitoseriu, L.; Buscaglia, V. Role of microstructures in the dielectric properties of PVDF-based nanocomposites containing high permittivity for energy storage. *Appl. Mater. Interfaces* **2023**, *15*, 13535–13544. [CrossRef]
67. Sousa, R.E.; Ferreira, J.C.C.; Costa, C.M.; Machado, A.V.M.; Silva, M.; Lanceros-Mendez, S. Tailoring poly (vinylidene fluoride-co-chlorotrifluoroethylene) microstructure and physicochemical properties by exploring its binary phase diagram with dimethylformamide. *J. Polym. Sci. Part B Polym. Phys.* **2015**, *53*, 761–773. [CrossRef]
68. Xiao, J.; Berlin, H.Z.; Zhou, X.; Zhang, Q.; Dowben, P.A. The effect of defects on the electronic structure of long chain ferroelectric polymers. *J. Appl. Phys.* **2009**, *106*, 044105. [CrossRef]
69. Zhang, S.; Tong, W.; Wang, J.; Wang, W.; Wang, Y.; Zhang, Y. Modified sepiolite/PVDF-HFP composite film with enhanced piezoelectric and dielectric properties. *J. Appl. Polym. Sci.* **2020**, *37*, 48412. [CrossRef]
70. Singh, B.; Kumar, R.; Cohan, J.S. Polymer matrix composites in 3D printing: A state of art review. *Mater. Today Proc.* **2020**, *33*, 1562–1567. [CrossRef]
71. Apelt, S.; Hohne, S.; Mehner, E.; Bohm, C.; Malanin, M.; Eichhorn, K.; Jehnichin, D.; Uhlmann, P.; Bergmann, U. Poly (vinylidene fluoride-co-trifluoroethylene) thin films after dip and spin coating. *Macromol. Mater. Eng.* **2022**, *307*, 220296. [CrossRef]
72. Lee, J.H.; Yoon, H.J.; Kim, T.Y.; Gupta, M.K.; Lee, J.H.; Seung, W.; Ryu, H.; Kim, S.W. Micropatterned P(VDF-TrFE) Film-Based Piezoelectric Nanogenerators for Highly Sensitive Self-Powered Pressure Sensors. *Adv. Funct. Mater.* **2015**, *25*, 3203–3209. [CrossRef]
73. Muduli, S.P.; Lipsa, L.; Choudhary, A.; Rajput, S.; Parida, S. Modulation of Electrical Characteristics of Polymer-Ceramic-Graphene Hybrid Composite for Piezoelectric Energy Harvesting. *ACS Appl. Electron. Mater.* **2023**, *5*, 3023–3037. [CrossRef]
74. Mahdi, R.I.; Gan, W.C.; Majid, W.H.A.; Mukri, N.I.; Furukawa, T. Ferroelectric polarization and pyroelectric activity of functionalized P(VDF-TrFE) thin film lead free nanocomposites. *Polymer* **2018**, *141*, 184–193. [CrossRef]
75. Koner, S.; Deshmukh, P.; Ahlawat, A.; Karnal, A.K.; Satapathy, S. Studies on structural, dielectric, impedance spectroscopy and magnetodielectric properties of La<sub>0.7</sub>Ba<sub>0.3</sub>MnO<sub>3</sub>/P(VDF-TrFE) multiferroic (0–3) nanocomposite films. *J. Alloys Compd.* **2021**, *868*, 159104. [CrossRef]
76. Mahdi, R.I.; Gan, W.C.; Halim, N.A.; Velayutham, T.S.; Majid, W.H.A. Ferroelectric and pyroelectric properties of novel Poly (vinylidene fluoride-trifluoroethylene-Bi<sub>0.5</sub>Na<sub>0.5</sub>TiO<sub>3</sub> nanocomposite films for sensing applications. *Ceram. Int.* **2015**, *41*, 13836–13843. [CrossRef]
77. Sebastian, M.T.; Jantunen, H. Polymer-Ceramic Composites of 0-3 connectivity for circuits in electronics: A review. *Int. J. Appl. Ceram. Technol.* **2010**, *7*, 415–434. [CrossRef]
78. Uchino, K. 9-Piezoelectric composite materials. In *Advanced Piezoelectric Material*; Uchino, K., Ed.; Woodhead Publishing: Swaston, UK, 2010; pp. 318–346.
79. Mameri, F. Chapter 3—Nanostructured flexible PVDF and fluoropolymer—Based hybrid films. In *Frontiers of Nanoscience*; Benelmekki, M., Erbe, A., Eds.; Elsevier: Amsterdam, The Netherlands, 2021; Volume 14, pp. 67–101.
80. Spin Coating Overview. Available online: [www.costeffectivetequipment.com/servicesupport/technical-resources/spincoating-theory](http://www.costeffectivetequipment.com/servicesupport/technical-resources/spincoating-theory) (accessed on 4 January 2023).
81. Xia, K.; Li, Y.C.; Li, J.; Xie, B.; Zhao, C. Research on the effect of spin coating process on ferroelectric phase of P(VDF-TrFE)/ZnO film. In Proceedings of the IEEE Symposium on Piezoelectricity, Acoustic Waves and Applications, Xi'an, China, 27–30 October 2017; IEEE: Piscataway, NJ, USA, 2017.
82. Dahan, R.; Arshad, A.N.; Razif, M.H.M.; Zohdi, N.S.N. Structural and electrical properties of PVDF-TrFE/ZnO bilayer and filled PVDF-TrFE/ZnO single layer nanocomposite films. *Adv. Mater. Process. Technol.* **2017**, *3*, 300–307.
83. Lau, K.; Liu, Y.; Chen, H.; Withers, R.L. Effect of annealing temperature on the morphology and piezoresponse characterization of poly(vinylidene fluoride-trifluoroethylene) films via scanning probe Microscopy. *Adv. Condens. Matter. Phys.* **2013**, *2013*, 435938. [CrossRef]
84. Rozana, M.D.; Wahid, M.H.; Arshad, A.N.; Sarip, M.N.; Habibah, Z.; Ismail, L.N.; Ruso, M. Effect of various annealing temperature on the morphological and dielectric properties of Polyvinylidene fluoride-Trifluoroethylene thin film. In Proceedings of the Symposium on Humanities Science and Engineering, Kuala Lumpur, Malaysia, 24–27 June 2012; IEEE: Piscataway, NJ, USA, 2012.
85. Men, T.; Liu, X.; Jiang, B.; Long, X.; Guo, H. Ferroelectric  $\beta$  crystalline phase formation and property enhancement in Poly-dopamine modified BaTiO<sub>3</sub>/PVDF-TrFE nanocomposite. *Thin Solid Film.* **2019**, *669*, 579–587. [CrossRef]
86. Chen, S.; Yao, K.; Tay, F.E.H.; Chew, L.L.S. Comparative investigation of the structure and properties of ferroelectric poly (vinylidene fluoride) and poly (vinylidene fluoride-trifluoroethylene) thin films crystallized on substrates. *J. Appl. Polym. Sci.* **2010**, *116*, 3331–3337. [CrossRef]

87. Park, Y.J.; Kang, S.J.; Shin, Y.; Kim, R.H.; Bae, I.; Park, C. Non-volatile memory characteristics of epitaxially grown PVDF-TrFE thin films and their printed micropattern application. *Curr. Appl. Phys.* **2011**, *11*, 30–34. [[CrossRef](#)]
88. Wahid, M.H.M. *The Doctoral Research Abstracts*; Institute of Graduate Studies, UiTM: Shah Alam, Malaysia, 2018.
89. Mai, M.; Zhu, C.; Liu, G.; Ma, X. Effect of dielectric layer on ferroelectric responses of P(VDF-TrFE) thin films. *Phys. Lett. A* **2018**, *382*, 2372–2375. [[CrossRef](#)]
90. Yang, J.H.; Ryu, T.; Lansac, Y.; Jang, Y.H. Shear stress-induced enhancement of the piezoelectric properties of PVDF-TrFE thin films. *Org. Electron.* **2016**, *28*, 67–72. [[CrossRef](#)]
91. Nguyen, V.; Rouxel, D.; Vincent, B.; Badie, L.; Santos, F.D.D.; Lamouroux, E.; Fort, Y. Influence of cluster size and surface functionalization of ZnO nanoparticles on the morphology, thermomechanical and piezoelectric properties of P(VDF-TrFE) nanocomposite films. *Appl. Surf. Sci.* **2013**, *279*, 204–211. [[CrossRef](#)]
92. Zhu, R.; Jenkins, K.; Yang, R. Degradation and Nano-Patterning of Ferroelectric P(VDF-TrFE) Thin Films with Electron Irradiation. *RSC Adv.* **2015**, *129*, 106700–106705. [[CrossRef](#)]
93. Zhang, Q.; Zhu, Z.; Shen, D.; Yang, H. Enhanced dielectric and hydrophobic properties of PDMS/P(VDF-TrFE) blend films by embedding PS microspheres. *Colloids Surf. A* **2019**, *569*, 171–178. [[CrossRef](#)]
94. Yaqoob, U.; Chung, G.S. Effect of surface treated MWCNTs and BaTiO<sub>3</sub> nanoparticle on the dielectric properties of a P(VDF-TrFE) Matrix. *J. Alloys Compod.* **2017**, *695*, 1231–1236. [[CrossRef](#)]
95. Fortunato, M.; Tamburrano, A.; Bracciale, M.P.; Santarelli, M.L.; Sarto, M.S. Enhancement of the piezoelectric coefficient in PVDF-TrFE/CoFe<sub>2</sub>O<sub>4</sub> nanocomposites through DC magnetic poling. *Beilstein J. Nanotechnol.* **2021**, *12*, 1262–1270. [[CrossRef](#)]
96. Wang, J.C.; Jiang, Y.P.; Lin, Y.J.; Chan, S.H. Trifluoroethylene bond enrichment in P(VDF-TrFE) copolymers with enhanced ferroelectric behaviors by plasma fluorination on bottom electrode. *J. Taiwan Inst. Chem. Eng.* **2020**, *107*, 152–160. [[CrossRef](#)]
97. Ahn, Y.; Son Yeog, J. Enhanced ferroelectric properties of P(VDF TrFE) thin films from Nb nano pin electrodes. *Polymer* **2019**, *180*, 121696. [[CrossRef](#)]
98. Perez, J.; Vilarinho, P.M.; Kholkin, A.L. High-quality PbZr<sub>0.52</sub>Ti<sub>0.48</sub>O<sub>3</sub> films prepared by modified sol-gel route at low temperature. *Thin Solid Films* **2004**, *449*, 20–24. [[CrossRef](#)]
99. Losego, M.D.; Ihlefeld, J.F.; Maria, J.P. Importance of solution chemistry in preparing sol-gel. *Chem. Mater.* **2008**, *20*, 303–307. [[CrossRef](#)]
100. Das, R.; Pattanayak, A.J.; Swain, S.K. *Polymer-Based Nanocomposites for Energy and Environmental Application*; Woodhead Publishing: Swaston, UK, 2018.
101. Galiano, F. Casting Solution. In *Encyclopedia of Membranes*; Drioli, E., Giorno, L., Eds.; Mannheim Media: New York, NY, USA, 2020.
102. Swain, S.K.; Pattanayak, A.J.; Sahoo, A.D. *Functional Biopolymers*; Thakur, V.K., Thakur, M.K., Eds.; Springer: Berlin/Heidelberg, Germany, 2017.
103. Koner, S.; Deshmukh, P.; Khan, A.A.; Ahlawat, A.; Karnal, A.K.; Satapathy, S. Multiferroic properties of La<sub>0.7</sub>Ba<sub>0.3</sub>MnO<sub>3</sub>/P(VDF-TrFE) (0-3) nano-composite films. *Mater Lett.* **2020**, *261*, 127161. [[CrossRef](#)]
104. Zhang, L.; Shan, X.; Wu, P.; Cheng, Z.-Y. Dielectric characteristics of CaCu<sub>3</sub>Ti<sub>4</sub>O<sub>12</sub>/P(VDF-TrFE) nanocomposites. *Appl. Phys. A* **2012**, *107*, 597–602. [[CrossRef](#)]
105. Bystrov, V.S.; Bdikin, I.K.; Kiselev, D.A.; Yudin, S.; Fridkin, V.M.; Kholkin, A.L. Nanoscale polarization patterning of ferroelectric Langmuir-Blodgett P(VDF-TrFE) films. *J. Phys. D Appl. Phys.* **2007**, *40*, 4571. [[CrossRef](#)]
106. Petty, M.; Tsibouklis, J.; Davis, F.; Hodge, P.; Petty, M.C.; Feast, W.J. Pyroelectric Langmuir-Blodgett films prepared using preformed polymers. *J. Phys. D Appl. Phys.* **1992**, *25*, 1032. [[CrossRef](#)]
107. Newnham, R.E. Properties of Materials. In *Anisotropy, Symmetry, Structure*; University Press: Oxford, NY, USA, 2004.
108. Breitenbach, J. Melt Extrusion: From process to drug delivery technology. *Eur. J. Pharm. Biopharm.* **2002**, *54*, 107–117. [[CrossRef](#)]
109. Nelson, K.D. Absorbable, drug-loaded, extruded fiber for implantation. In *Biomedical Textiles for Orthopedic and Surgical Applications*; Woodhead Publishing: Sawston, UK, 2005; pp. 119–143.
110. Meng, N.; Zhu, X.; Mao, R.; Reece, M.J.; Bilotti, E. Nanoscale Interfacial Electroactivity in PVDF/PVDF-TrFE Blended Films with Enhanced Dielectric and Ferroelectric. *J. Mater. Chem. C* **2017**, *13*, 3296–3305. [[CrossRef](#)]
111. Meng, N.; Ren, X. Multiscale understanding of electric polarization in PVDF based ferroelectric Polymers. *J. Mater. Chem. C* **2020**, *46*, 16436–16442. [[CrossRef](#)]
112. Beringar, L.T.; Xu, X.; Shih, W.; Shih, W.; Habas, R.; Schauer, C. An electrospun PVDF-TrFE fiber sensor platform for biological applications. *Sens. Actuators A* **2015**, *222*, 293–300. [[CrossRef](#)]
113. Kim, Y.; Wu, X.; Lee, C.; Oh, J.H. Characterization of PI/PVDF-TrFE composite nanofiber based Triboelectric nanogenerators depending on the type of the electrospinning system. *ASC Appl. Mater. Interfaces* **2021**, *13*, 31. [[CrossRef](#)] [[PubMed](#)]
114. Pourbafrani, M.; Azimi, S.; Nia, N.Y.; Zendehtdel, M.; Abolhasani, M.M. The effect of electrospinning parameters on piezoelectric PVDF-TrFE nanofibers: Experimental and simulation study. *Energies* **2023**, *16*, 37. [[CrossRef](#)]
115. Jiang, Y.G.; Sun, X.J.; Zhang, D.Y. Highly aligned P(VDF-TrFE) nano fibers with anisotropic piezoelectricity fabricated by electrospinning for physical sensing device. In Proceedings of the IEEE International Conference on Solid State Sensors, Actuators and Micro Systems, Anchorage, AK, USA, 21–25 June 2015; IEEE: Piscataway, NJ, USA, 2015.

116. Ico, G.; Showalter, A.; Bosze, W.; Gott, S.C.; Kim, B.S.; Rao, M.P.; Myung, N.V.; Nam, J. Size dependent piezoelectric and mechanical properties of electrospun P(VDF-TrFE) nanofibers for enhanced energy harvesting. *J. Mater. Chem. A* **2016**, *4*, 2293–2304. [[CrossRef](#)]
117. Kibria, F.; Rahman, W. Electrospinning based high sensitive PVDF-TrFE nanofiber sensor with sensitivity dependence on pore diameter. *Curr. Sci.* **2020**, *119*, 5. [[CrossRef](#)]
118. Ahmed, A.; Jia, J.; Huang, Y.; Khoso, N.A.; Deb, H.; Fan, Q.; Shao, J. Preparation of PVDF-TrFE based electrospun nanofibers decorated with PEDOT-CNT/rGO Composites for piezo electric pressure sensor. *J. Mater. Sci. Mater. Electron.* **2019**, *30*, 14007–14021. [[CrossRef](#)]
119. Kang, H.B.; Han, C.S.; Pyun, J.C.; Ryu, W.H.; Kang, C.Y.; Cho, Y.S. (Na, K)NbO<sub>3</sub> nanoparticle-embedded piezoelectric nanofiber composites for flexible nanogenerators. *Compos. Sci. Technol.* **2015**, *111*, 1–8. [[CrossRef](#)]
120. Liu, K.; Choi, H.J.; Kim, B.K.; Kim, D.B.; Han, C.S.; Kim, S.W.; Kang, H.B.; Park, J.W.; Chao, Y.S. Piezoelectric energy harvesting and charging performance of Pb(Zn<sub>1/3</sub>Nb<sub>2/3</sub>)O<sub>3</sub>-Pb(Zr<sub>0.5</sub>Ti<sub>0.5</sub>)O<sub>3</sub> nanoparticle-embedded P(VDF-TrFE) nanofiber composite sheets. *Compos. Sci. Technol.* **2018**, *168*, 296–302. [[CrossRef](#)]
121. Liu, J.; Yang, B.; Lu, L.; Wang, X.; Li, X.; Chen, X.; Liu, J. Flexible and lead-free piezoelectric nanogenerator as self-powered sensor based on electro spinning BZT-BCT/P(VDF-TrFE)nanofibers. *Sens. Actuators A* **2020**, *303*, 111796. [[CrossRef](#)]
122. Wang, X.; Yang, B.; Liu, J.; Zhu, Y.; Yang, C.; He, Q. A flexible triboelectric piezoelectric hybrid nanogenerator based on PVDF-TrFE nanofibers and PDMS/MWCNT for wearable device. *Sci. Rep.* **2006**, *6*, 36409. [[CrossRef](#)]
123. Turdakyn, N.; Bekezhankyzy, Z.; Araby, S.; Montazami, R.; Bakenov, Z.; Kalimuldina, G. Investigation of electrospun piezoelectric P(VDF-TrFE) nanofiber-based nanogenerators for energy harvesting. *Energy Rep.* **2023**, *10*, 628–636. [[CrossRef](#)]
124. Serairi, L.; Gu, L.; Qin, Y.; Lu, Y.; Basset, P.; Wang, Y.L. Flexible piezoelectric nanogenerators based on PVDF-TrFE nanofibers. *Eur. Phys. J. Appl. Phys.* **2017**, *80*, 30901. [[CrossRef](#)]
125. Topark, A.; Tigil, O. Micron scale energy harvesters using multiple piezoelectric polymer layers. *Sens. Actuators A* **2018**, *269*, 412–418. [[CrossRef](#)]
126. Kim, S.; Towfeeq, I.; Dong, Y.; Gorman, S.; Rao, A.M.; Koley, J. P(VDF-TrFE) Film on PDMS Substrate for Energy Harvesting Applications. *Appl. Sci.* **2018**, *8*, 213. [[CrossRef](#)]
127. Habibur, R.M.; Yaqoob, U.; Muhammad, S.; Uddin, A.S.M.; Kim, H.C. The effect of RGO on dielectric and energy harvesting properties of P(VDF-TrFE) matrix by optimizing electro active  $\beta$  phase without traditional polling process. *Mater. Chem. Phys.* **2018**, *215*, 46–55. [[CrossRef](#)]
128. Kim, Y.; Kim, D.; Jung, J.; Kim, S.W.; Kim, M. Airflow induced P(VDF-TrFE) fiber arrays for enhanced piezoelectric harvesting. *APL Mater.* **2022**, *10*, 031110. [[CrossRef](#)]
129. Kullukcu, B.; Beker, L. Design and modeling of a PVDF-TrFE flexible wind energy harvesters. *Turk. J. Electr. Eng. Comput. Sci.* **2023**, *31*, 6. [[CrossRef](#)]
130. Zhang, Q.Q.; Chan, H.L.W.; Ploss, B.; Choy, C.L. PCLT/P(VDF-TrFE) nanocomposite pyroelectric sensors. *IEEE Trans. Ultrason. Ferroelectr. Freq. Control* **2001**, *48*, 154–160. [[CrossRef](#)]
131. Wang, S.; Shao, H.Q.; Liu, Y.; Tang, C.Y.; Zhao, X.; Ke, K.; Bao, R.K.; Yang, M.B.; Yang, W. Boosting piezoelectric response of PVDF-TrFE via Mxene for self-powered linear pressure sensor. *Compos. Sci. Technol.* **2021**, *202*, 108600. [[CrossRef](#)]
132. Gupta, S.; Shakthivel, D.; Lorenzelli, L.; Dahiya, R. Temperature compensated tactile sensing using MOSFET with PVDFTrFE/BaTiO<sub>3</sub> capacitor as extended gate. *IEEE. Sens. J.* **2019**, *19*, 435–442. [[CrossRef](#)]
133. Nazir, N.A.; Kim, N.; Iglesias, W.G.; Jakli, A.; Kyu, T. Conductive behavior in relation to domain morphology and phase diagram of Nafion/poly (vinylidene-co-trifluoroethylene) blends. *Polymer* **2012**, *53*, 196–204. [[CrossRef](#)]
134. Simoes, R.D.; Rodriguez-Perez, M.A.; De Saja, J.A.; Constantino, C.J.L. Tailoring, the structural properties of PVDF and P(VDF-TrFE) by using natural polymers as additives. *Poly. Eng. Sci.* **2009**, *49*, 2150–2157. [[CrossRef](#)]
135. Li, Y.; Liao, C.; Tjnog, S.C. Electrospun polyvinylidene fluoride based fibrous scaffolds with piezoelectric characteristics for bone and neural tissue engineering. *Nanomaterials* **2019**, *9*, 952. [[CrossRef](#)] [[PubMed](#)]
136. Orkwis, J.A.; Wolf, A.K.; Mularczyk, Z.J.; Bryan, A.E.; Smith, C.S.; Brown, R.; Krutko, M.; McCann, A.; Collar, R.M.; Esfandiari, L.; et al. Mechanical stimulation of a bioactive, functionalized PVDF-TrFE scaffold provides electrical signaling for nerve repair application. *Biomater. Adv.* **2022**, *140*, 213081. [[CrossRef](#)] [[PubMed](#)]
137. Adadi, N.; Yadid, M.; Gai, I.; Asulin, M.; Feiner, R.; Edri, R.; Dvir, T. Electrospun fibrous PVDF-TrFE scaffolds for cardiac tissue engineering, differentiation and maturation. *Adv. Mater. Technol.* **2020**, *5*, 1900820. [[CrossRef](#)]
138. Ohigashi, H.; Koyama, H.K.; Takahashi, S.; Ishizaki, A.; Maida, Y. Piezoelectric Properties of P(VDF-TrFE) Thin Films at Low Temperatures and Their Application to Ultrasonic Transducers for Scanning Acoustic Microscopy Operating in a Wide Temperature Range. *Jpn. J. Appl. Phys.* **1989**, *28*, 28–66. [[CrossRef](#)]
139. Ducrot, P.H.; Dufour, I.; Ayela, C. Optimization of PVDF-TrFE Processing Conditions for The Fabrication of Organic MEMS Resonators. *Sci. Rep.* **2016**, *6*, 19426. [[CrossRef](#)]
140. Kanek, R.; Froemel, J.; Tanaka, S. Development of PVDF-TrFE/SiO<sub>2</sub> composite film bulk acoustic resonator. *Sens. Actuator A* **2018**, *284*, 120–128. [[CrossRef](#)]
141. Takahashi, S. Properties and characteristics of P(VDF/TrFE) transducers manufactured by a solution casting method for use in the MHz-range ultrasound in air. *Ultrasonics* **2012**, *52*, 422–426. [[CrossRef](#)]

142. Jung, S.W.; Yoon, S.M.; Kang, S.Y.; You, I.K.; Koo, J.B.; Baeg, K.J.; Noh, Y.Y. Low-voltage-operated top-gate polymer thin-film transistors with high-capacitance P(VDF-TrFE)/PVDF-blended dielectrics. *Curr. Appl. Phys.* **2011**, *11*, S213–S218. [[CrossRef](#)]
143. Sahoo, R.; Mishra, S.; Unnikrishnan, L.; Mohanty, S.; Mahapatra, S.; Nayak, S.K.; Anwar, L.; Ramadoss, A. Enhanced dielectric and piezoelectric properties of Fe doped ZnO/PVDF-TrFE composite films. *Mater. Sci. Semicond. Process* **2020**, *117*, 105173. [[CrossRef](#)]
144. Sahoo, R.; Mishra, S.; Ramadoss, A.; Mohanty, S.; Mahapatra, S.; Nayak, S.K. An approach towards the fabrication of energy harvesting device using Ca doped ZnO/PVDF-TrFE composite film. *Polymer* **2020**, *205*, 122869. [[CrossRef](#)]
145. Kim, J.H.; Kim, B.; Kim, S.W.; Kang, H.W.; Park, M.C.; Park, D.H.; Ju, B.K.; Choi, W.K. High performance coaxial piezoelectric energy generator (C-PEG) yarn of Cu/PVDF-TrFE/PDMS/Nylon/Ag. *Nanotechnology* **2021**, *32*, 145401. [[CrossRef](#)] [[PubMed](#)]
146. Aliane, A.; Benwadih, M.; Bouthinon, B.; Coppard, R.; Santos, F.D.D.; Daami, A. Impact of crystallization on ferro, piezo and pyro electric characteristics in thin film P(VDF-TrFE). *Org. Electron.* **2015**, *25*, 92–98. [[CrossRef](#)]
147. Gosh, S.K.; Roy, K.; Mishra, H.K.; Sahoo, M.R.; Mohanty, B.; Vishwakarma, P.N.; Mandal, D. Rollable Magnetolectric energy harvesters as wireless IOT sensor. *ACS Sustain. Chem. Eng.* **2020**, *8*, 864–873. [[CrossRef](#)]
148. Sun, Q.Q.; Xia, W.M. The dependence of acoustic emission on the crystal structures, dielectric, ferroelectric and piezoelectric properties of P(VDF-TrFE) sensors. *IEEE Trans. Ultrason. Ferroelectro. Freq. Control* **2020**, *67*, 975–983. [[CrossRef](#)]
149. Wen, D.; Chen, X.; Huang, F.; Zhang, J.; Yang, P.; Li, R.; Lu, Y.; Liu, Y. Piezoelectric and magnetoelectric effects of flexible magnetoelectric heterostructure PVDF-TrFE/FeCoSiB. *Int. J. Mol. Sci.* **2022**, *23*, 15992. [[CrossRef](#)]
150. Ummer, R.P.; Raneesh, B.; Thevenot, C.; Rouxel, D.; Thomas, S.; Kalarikkal, N. Electric, Magnetic, Piezoelectric and Magnetolectric studies of phase pure (BiFeO<sub>3</sub>-NaNbO<sub>3</sub>)-P(VDF-TrFE) nanocomposites prepared by spin coating. *RSC Adv.* **2016**, *6*, 28069–28080. [[CrossRef](#)]
151. Li, J.W.; Huang, C.Y.; Chen, K.Y.; Chen, J.X.; Hsu, X.Y.; Chen, Y.F.; Kuo, C.F.J.; Cheng, C.C.; Snen, M.C.; Chiu, C.W. Enhanced piezoelectric properties of poly(vinylidene fluoride-co-trifluoroethylene)/carbon based nanomaterial composite films for pressure sensing application. *Polymers* **2020**, *12*, 2999. [[CrossRef](#)]
152. Yao, L.; Zhang, Z.; Zhang, Q.; Zhou, Z.; Yang, H.; Chen, L. Modified organic polystyrene microspheres embedded into PVDF-TrFE with lotus leaf microstructure enables high performance triboelectric nanogenerator. *Nano Energy* **2021**, *86*, 106128. [[CrossRef](#)]
153. Wang, A.; Hu, M.; Zhou, L.; Qiang, X. Self powered well aligned PVDF-TrFE piezoelectric nanofiber nanogenerator for modulating an exact electrical stimulation and enhancing the proliferation of preosteoblasts. *Nanomaterials* **2019**, *9*, 349. [[CrossRef](#)] [[PubMed](#)]
154. Jiang, Y.P.; Yang, T.C.; Lin, T.H.; Ho, C.M.; Chan, S.H.; Wu, M.C.; Wang, J.C. Layer dependent solvent vapor annealing on stacked ferroelectric PVDF-TrFE copolymers for highly efficient nanogenerator applications. *Polymer* **2020**, *204*, 122822. [[CrossRef](#)]
155. Han, J.; Kim, J.H.; Choi, H.J.; Kim, S.W.; Sung, S.M.; Kim, M.S.; Choi, B.K.; Paik, J.H.; Lee, J.S.; Cho, Y.S. Origin of enhanced piezoelectric energy harvesting in all polymer based core shell nanofibers with controlled shell thickness. *Compos. Part B* **2021**, *223*, 109141. [[CrossRef](#)]
156. Hernandez, N.; Gonzalez, V.G.; Bautista, D.; Soto, N.O.; Barandiaran, J.M.; Gutierrez, J. Electrospun poly (vinylidene fluoride-trifluoroethylene) based flexible magnetoelectric nanofibers. *Eur. Polym. J.* **2018**, *109*, 336–340. [[CrossRef](#)]
157. Toprak, A. MEMS Scale PVDF-TrFE based piezoelectric energy harvesters. *J. Microelectromech. Syst.* **2015**, *24*, 1989–1997. [[CrossRef](#)]
158. Toprak, A.; Tigli, O. Comprehensive characterization of PVDF-TrFE thin films for microelectromechanical system application. *J. Mater. Sci. Mater. Electron.* **2017**, *28*, 15877–15885. [[CrossRef](#)]
159. Hu, X.; You, M.; Yi, N.; Zhang, X.; Xiang, Y. Enhanced piezoelectric coefficient of PVDF-TrFE films via in situ polarization. *Front. Energy Res.* **2021**, *9*, 621540. [[CrossRef](#)]
160. Ahn, G.; Kim, S.R.; Choi, Y.-Y.; Song, H.W.; Sung, T.H.; Hong, J.; No, K. Facile preparation of ferroelectric poly (vinylidene fluoride co trifluoroethylene) thick films by solution casting. *Polym. Eng. Sci.* **2014**, *54*, 466–471. [[CrossRef](#)]
161. Disnan, D.; Hafner, J.; Schneider, M.; Schmid, U. Spherulite like microstructure observed for spin cast P(VDF-TrFE) thin films and their ferroelectric characterization. *Polymer* **2023**, *272*, 125840. [[CrossRef](#)]

**Disclaimer/Publisher's Note:** The statements, opinions and data contained in all publications are solely those of the individual author(s) and contributor(s) and not of MDPI and/or the editor(s). MDPI and/or the editor(s) disclaim responsibility for any injury to people or property resulting from any ideas, methods, instructions or products referred to in the content.